中国光学 Chinese Optics 核心期刊

高效率蓝光硅光探测器外延结构及特性研究

陈伟帅 王浩冰 陶金 高丹 吕金光 秦余欣 郭广通 李香兰 王强 张军 梁静秋 王惟彪

A study on the epitaxial structure and characteristics of high-efficiency blue silicon photodetectors

CHEN Wei-shuai, WANG Hao-bing, TAO Jin, Gao Dan, LV Jin-guang, QIN Yu-xin, GUO Guang-tong, LI Xiang-lan, WANG Qiang, ZHANG Jun, LIANG Jing-qiu, WANG Wei-biao

引用本文:
陈伟帅, 王浩冰, 陶金, 高丹, 吕金光, 秦余欣, 郭广通, 李香兰, 王强, 张军, 梁静秋, 王惟彪. 高效率蓝光硅光探测器外延结构及特性研究[J]. 中国光学, 2022, 15(3): 568–591. doi: 10.37188/CO.2021–0188
CHEN Wei-shuai, WANG Hao-bing, TAO Jin, Gao Dan, LV Jin-guang, QIN Yu-xin, GUO Guang-tong, LI Xiang-lan, WANG Qiang, ZHANG Jun, LIANG Jing-qiu, WANG Wei-biao. A study on the epitaxial structure and characteristics of high-efficiency blue silicon photodetectors[J]. *Chinese Optics*, 2022, 15(3): 568-591. doi: 10.37188/CO.2021-0188

在线阅读 View online: https://doi.org/10.37188/CO.2021–0188

文章编号 2095-1531(2022)03-0568-24

A study on the epitaxial structure and characteristics of high-efficiency blue silicon photodetectors

CHEN Wei-shuai[1,2†], WANG Hao-bing[1,2†], TAO Jin[1], Gao Dan[1], LV Jin-guang[1], QIN Yu-xin[1], GUO Guang-tong[1,2], LI Xiang-lan[1,2], WANG Qiang[1], ZHANG Jun[3], LIANG Jing-qiu[1 *], WANG Wei-biao[1 *]

(1. *State Key Laboratory of Applied Optics*, *Changchun Institute of Optics*, *Fine Mechanics and Physics*, *Chinese Academy of Sciences*, *Changchun* 130033, *China*;

2. *University of Chinese Academy of Sciences*, *Beijing* 100049, *China*;

3. *Collage of Science* & *Engineering*, *Jinan University*, *Guangzhou Key Laboratory of Visible Light Communication Engineering Technology*, *Guangzhou* 510632, *China*)

† *These authors contribute equally*

* *Corresponding author*, *E-mail*: *liangjq@ciomp.ac.cn*; *wangwb@ciomp.ac.cn*

Abstract: In order to achieve high spectral responsivity of the silicon avalanche photodiode in blue band (400−500 nm), Separated Absorption Control Multiplication (SACM) basic device structure was designed. Based on multiple physical models, the effect of the thickness on the avalanche breakdown voltage and the photocurrent gain of the device and the effect of the doping concentration of the multiplication layer on the optical responsivity were investigated. Comprehensively considering the factors of light responsivity and breakdown voltage, the results show that the device has a low breakdown voltage $V_{\text{br-apd}}$=34.2 V when the doping concentration of the surface non-depleted layer is 1.0×10^{18} cm^{-3}, and the thickness is 0.03 μm; the doping concentration of absorption layer is 1.0×10^{15} cm^{-3}, the thickness is 1.3 μm, the doping concentration of field control layer is 8.0×10^{16} cm^{-3}, the thickness is 0.2 μm and the doping concentration of double layer is 1.8×10^{16} cm^{-3} and the thickness is 0.5 μm. When $V_{\text{apd}}=0.95V_{\text{br-apd}}$, it has higher optical responsivity in blue band, i.e. *SR* is 3.72~6.08 A·W^{-1}. The above research results provide certain theoretical reference for the preparation of practical Si-APD devices with high blue light detection responsivity.

Key words: avalanche photodiode; silicon; spectral response

收稿日期:2021-11-01; 修订日期:2021-12-07

基金项目:国家重点研发计划(No. 2018YFB1801902, No. 2018YFB1801901, No. 2019YFB2006003);吉林省科技发展计划项目(No. 20190302062GX);国家自然科学基金(青年基金)(No. 12004139);广东省科技计划项目资助项目(No. 2016B010111003)

Supported by National Key Research and Development Program (No. 2018YFB1801902, No. 2018YFB1801901, No. 2019YFB2006003); Science and Technology Development Program Project (No. 20190302062GX); Youth Project of National Natural Science Foundation of China (NSFC) (No. 12004139); Science and Technology Plan Program Project of Guangdong Province (No. 2016B010111003)

高效率蓝光硅光探测器外延结构及特性研究

陈伟帅[1,2†], 王浩冰[1,2†], 陶 金[1], 高 丹[1], 吕金光[1], 秦余欣[1], 郭广通[1,2],
李香兰[1,2], 王 强[1], 张 军[3], 梁静秋[1*], 王惟彪[1*]
(1. 中国科学院长春光学精密机械与物理研究所, 应用光学国家重点实验室, 长春 130033;
2. 中国科学院大学, 北京 100049;
3. 暨南大学理工学院, 广州市可见光通信工程技术重点实验室, 广州 510632)
† 共同贡献作者

摘要: 为了实现硅基雪崩光电二极管蓝光波段(400~500 nm)高光响应度, 设计了 SACM 型基本器件结构, 探究了倍增层厚度对器件的雪崩击穿电压及光电流增益的影响及倍增层掺杂浓度对光响应度的影响, 综合考虑光响应度和击穿电压的因素, 结果表明: 当表面非耗尽层掺杂浓度为 1.0×10^{18} cm^{-3}、厚度为 0.03 μm; 吸收层掺杂浓度为 1.0×10^{15} cm^{-3}、厚度为 1.3 μm; 场控层掺杂浓度为 8.0×10^{16} cm^{-3}、厚度为 0.2 μm; 倍增层掺杂浓度为 1.8×10^{16} cm^{-3}、厚度为 0.5 μm 时, 器件具有较低的击穿电压 $V_{\text{br-apd}}$=34.2 V。当 V_{apd}=0.95 $V_{\text{br-apd}}$, 该结构在蓝光波段具较高的光响应度(SR=3.72~6.08 A·W^{-1})。上述研究结果对高蓝光探测响应度 Si-APD 实际器件的制备具有一定的参考价值。

关 键 词: 雪崩光电二极管; 硅; 光谱响应度
中图分类号: TP394.1;TH691.9 **文献标志码:** A **doi:** 10.37188/CO.2021-0188

1 Introduction

With the development and wide application of short-wavelength visible light sources (such as blue LEDs, blue semiconductor lasers), the application requirements of short-wavelength visible light efficient detection technology are also increasing. Especially with the rapid development of visible light communication technology[1], biomedical engineering, underwater optical communication[2] and other fields, there is an urgent need for visible light detectors with high bandwidth, high gain, wide spectrum and high optical response[3]. White LEDs are an important light source for visible light communication[4]. Currently, commonly used white LEDs mainly include fluorescent white LEDs (white light is formed by mixing phosphors excited by blue LEDs to form white light[5]); red, green and blue white LEDs (RGB-LED)[6]. For the above two white LEDs, blue light is the main working band, so photodetectors with high blue light response are of great significance to further promote the development and application of the integration of lighting and communication[7]. Currently commonly used photodetectors are mainly PIN photodiode (PIN-PD), Photo Multiplier Tube (PMT) and Avalanche Photodiode (APD). However, PIN has low optical responsivity, short detection distance, and high light source power requirements, which limit its further application in visible light communication[8]. PMTs can detect short wavelengths, but the disadvantages of high voltage and sensitivity to magnetic fields limit their application in visible light communication[9]. Avalanche photodetector (APD) is a semiconductor detector with high internal gain and high photoresponsivity[10], and does not have the above-mentioned disadvantages of PMT, so it has attracted extensive attention in the research of visible light detectors.

Silicon (Si) can absorb incident light in the 380–1 100 nm band, which is a good material for the preparation of wide-spectrum detectors[11]. In addition, the preparation process of Si semiconductor devices is mature[12] and the impact ionization rate of electrons to holes is high and the tunnel current is low in silicon materials[13]. Therefore, the silicon-based avalanche photodiode (Si-APD) has the advantages of high gain, low noise and good stability. However, due to the high absorption coefficient of blue light in silicon, the penetration depth of blue light in silicon is relatively shallow, and most of the photo-generated carriers are located in the shallow surface layer. Therefore, it is easy to cause some carriers to recombine on the shallow surface, resulting in a small number of photogenerated carriers entering the absorption layer and low photoelectric conversion efficiency in the blue light band. This brings great difficulty to the design and fabrication of Si-APD device with high blue light responsivity. In order to improve the detection efficiency of silicon for blue light and to improve the performance of Si-APD in the blue light band, researchers have carried out the following related studies: in 2010, Catherine M. Pepin *et al.* of Excelitas Company prepared a UV-enhanced Si-based APD by "buried junction" on an epitaxial wafer with an avalanche breakdown voltage of 400 V and a responsivity of 39 A/W (M=150) at a wavelength of 430 nm[14]. In 2015, Othman *et al.* highly integrated Si-based APDs through a CMOS process with an avalanche breakdown voltage of 10 V and a gain of 100 at 405 nm wavelength[15]. In the same year, Wang Xudong *et al.* optimized the structural parameters of the device based on Separated Absorption Control Multiplication (SACM) type Si-APD (n-p-p$^+$-p-p$^+$ type doped structure, light incident from the surface of the N type layer), and an antireflective film structure with alternating high and low refractive index was designed on the device surface. With the structure of antireflection coating, the optimized device has a peak response wavelength of 406 nm, avalanche breakdown voltage of 105.9 V, and optical responsivity at the peak wavelength of 250 A/W[16]. In 2015, Huo Linzhang *et al.* proposed a SiPM detector with a deep trench isolation structure, which improved the detection efficiency in the blue-violet region (360~420 nm) with about 90 V of the breakdown voltage[17]. In 2019, Lu Huanhuan *et al.* designed a SAM-type Si-APD. The multiplication layer of the device is closer to the photosensitive layer, which can effectively reduce the recombination loss of photogenerated carriers. The device has a breakdown voltage of about 50 V and a photoresponsivity of 31.1 A/W at 450 nm[18]. In the above studies, the blue light detection efficiency of Si-APD devices was improved. With the increasing demand, it is necessary to further study Si-APD devices to improve their blue light detection performance. Conventional Si-APD devices generally have a higher avalanche breakdown voltage V_{br} (150~500 V) which makes the device power consumption larger and the stability worse. In order to obtain high blue light responsivity and low avalanche breakdown voltage of Si-APD devices in blue light band, based on the traditional Si-APD structure, according to the transport characteristics of photogenerated carriers, a structure in which the positions of the absorption layer and the avalanche layer are interchanged is designed, and the structure is optimized in the blue light band. The relationship between the doping concentration and thickness of the device multiplication layer and the avalanche breakdown voltage and spectral responsivity is also studied. This paper provides a basic reference for the design and fabrication of practical high blue light responsivity silicon-based avalanche photodetector chips.

2 Epitaxial structure design

2.1 SACM type Si-APD

According to the analysis of the visible light absorption characteristics of Si (The material parameters of Si used in this paper are from the experimental measurements of Schinke *et al*[19]) and that of the working principle of the Si avalanche photodetector, a SACM device structure is adopted, that is, the absorption layer and the multiplication layer are separated, a field control layer is added between them, and the multiplication layer is placed behind[20-21]. The basic epitaxial structure of SACM type Si-APD is shown in Fig. 1 (color online) from top to bottom, the device is a p^{++} type heavily doped surface non-depletion layer, a π type absorption layer, a p$^+$field control layer, a p type multiplication layer and an n^{++} type substrate. Light is incident from the surface of the p^{++} non-depletion layer. The absorption layer can absorb incident light with a wavelength of 0.3 to 1.1 μm, covering the visible light band, the field control layer is used to modulate the electric field between the multiplication layer and the absorption layer in the device to achieve a good transition between the low electric field intensity of the absorption layer and the high electric field intensity of the multiplication layer. Under the premise of ensuring that the photogenerated carriers can be transported to the avalanche layer, the noise carriers can be suppressed[22]. The multiplication layer is used to achieve the number gain of the initial photogenerated carriers; the surface non-depletion layer and the heavily doped substrate act as conductive electrode. When the applied bias voltage is high enough, the device will be in a pull-through state, that is, from the PN junction to the surface non-depletion layer, the depletion region not only ensures the avalanche breakdown of the multiplication layer, but also ensures that the electric field of the absorption layer is high enough, so that the photogenerated carriers can reach the saturation drift velocity and move to the multiplication layer.

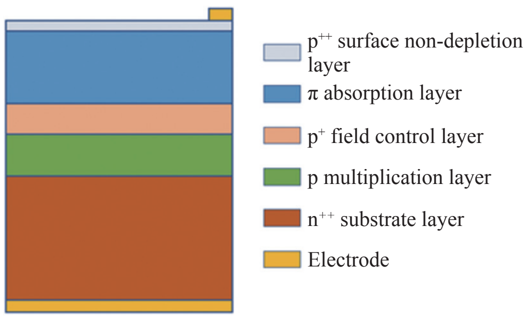

Fig. 1　The basic epitaxial structure of SACM type Si-APD

图 1　SACM-APD 基本外延结构

2.2　Electric field distribution in Si-APD

The electric field distribution of the PN junction depletion layer can be expressed as

$$E(x) = E_M - \frac{qN_m}{\varepsilon_0\varepsilon_m}x \quad , \qquad (1)$$

where q is the single charge, N_m is the impurity concentration, ε_m is the relative permittivity of the doping material, ε_0 is the vacuum permittivity, E_M is the maximum electric field strength in the PN junction, and E_M is related on the doping concentration on both sides of the multiplication layer and the applied bias voltage V_m, expressed as

$$E_M = \left[\frac{2q(V_m + V_{bi})}{\varepsilon_0\varepsilon_m}\cdot\frac{N_A N_D}{N_A + N_D}\right]^{\frac{1}{2}} \quad , \qquad (2)$$

where N_D is the donor impurity concentration, N_A is the acceptor impurity concentration, and V_{bi} is the built-in potential of the multiplication layer, expressed as:

$$V_{bi} = \frac{KT}{q}\ln\left(\frac{N_A N_D}{n_i^2}\right) \quad , \qquad (3)$$

where K is the Boltzmann constant, T is the Kelvin temperature (T=300 K), and n_i is the intrinsic carrier concentration (n_i=1.02×10^{10}cm^{-3}[23]).

According to formula (1), the expression of electric field of each layer of the device in Fig.2 (color online) is deduced (the built-in potential of homogeneous junction due to different doping concentration is not considered in this paper).

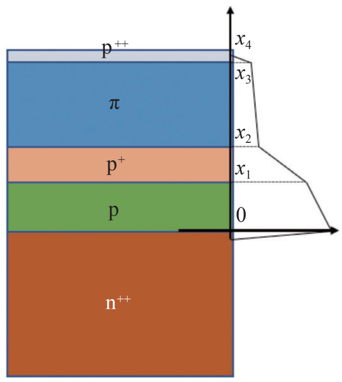

Fig. 2　The distribution of electric field in Si-APD

图 2　Si 基 APD 内部电场分布

when $0 < x < x_1$,

$$E(x) = E_M - \frac{qN_p}{\varepsilon_0\varepsilon_p}x \quad , \qquad (4)$$

when $x_1 < x < x_2$,

$$E(x) = E_M - \frac{qN_p}{\varepsilon_0\varepsilon_p}x_1 - \frac{qN_{p+}}{\varepsilon_0\varepsilon_{p+}}x \quad , \qquad (5)$$

when $x_2 < x < x_3$,

$$E(x)=E_{\mathrm{M}}-\frac{qN_{\mathrm{p}}}{\varepsilon_0\varepsilon_{\mathrm{p}}}x_1-\frac{qN_{\mathrm{p+}}}{\varepsilon_0\varepsilon_{\mathrm{p+}}}x_2-\frac{qN_{\pi}}{\varepsilon_0\varepsilon_{\pi}}x \quad , \tag{6}$$

when $x_3 < x < x_4$,

$$E(x)=E_{\mathrm{M}}-\frac{qN_{\mathrm{p}}}{\varepsilon_0\varepsilon_{\mathrm{p}}}x_1-\frac{qN_{\mathrm{p+}}}{\varepsilon_0\varepsilon_{\mathrm{p+}}}x_2-\frac{qN_{\pi}}{\varepsilon_0\varepsilon_{\pi}}x_3-\frac{qN_{\mathrm{p++}}}{\varepsilon_0\varepsilon_{\mathrm{p++}}}x \quad , \tag{7}$$

where N_{p}, $N_{\mathrm{p+}}$, N_{π} and $N_{\mathrm{p++}}$ are the doping concentrations of the multiplication layer, field control layer, absorption layer and surface non-depletion layer, respectively. By modulating the doping concentration and thickness of each layer, the electric field distribution and corresponding voltage in each layer can be designed and modulated; E_{M} is the electric field strength at the position of x = 0 in Fig. 2, which is also the maximum electric field strength in the device; ε_{p}, $\varepsilon_{\mathrm{p+}}$, ε_{π} and $\varepsilon_{\mathrm{p++}}$ represent the relative permittivity of the multiplication layer, field control layer, absorption layer and surface non-depletion layer. The relative permittivity of doped silicon[24] can be expressed as:

N-type doped silicon:

$$\varepsilon_{\mathrm{Si}}(N_{\mathrm{D}})=\frac{1.635\times10^{-19}N_{\mathrm{D}}}{1+1.172\times10^{-21}N_{\mathrm{D}}}+11.688 \quad , \tag{8}$$

P-type doped silicon:

$$\varepsilon_{\mathrm{Si}}(N_{\mathrm{A}})=\frac{1.5\times10^{-16}N_{\mathrm{A}}}{105.3-4.9496\times10^{-5}N_{\mathrm{A}}^{1/3}-3.283\times10^{-18}N_{\mathrm{A}}}+11.7. \tag{9}$$

If the thickness and doping concentration of each layer are determined, according to the electric field distribution in the device defined by Equations (4)−(7), the voltage V_{apd} on the Si-APD device in Fig. 1 can be expressed as:

$$V_{apd}=V_{\mathrm{m}}+V_{\mathrm{c}}+V_{\mathrm{a}}=\int_0^{x_1}\left(E_{\mathrm{M}}-\frac{qN_{\mathrm{p}}}{\varepsilon_0\varepsilon_{\mathrm{p}}}x\right)\mathrm{d}x+\int_{x_1}^{x_2}\left(E_{\mathrm{M}}-\frac{qN_{\mathrm{p}}}{\varepsilon_0\varepsilon_{\mathrm{p}}}x_1-\frac{qN_{\mathrm{p+}}}{\varepsilon_0\varepsilon_{\mathrm{p+}}}x\right)\mathrm{d}x+\int_{x_2}^{x_3}\left(E_{\mathrm{M}}-\frac{qN_{\mathrm{p}}}{\varepsilon_0\varepsilon_{\mathrm{p}}}x_1-\frac{qN_{\mathrm{p+}}}{\varepsilon_0\varepsilon_{\mathrm{p+}}}x_2-\frac{qN_{\pi}}{\varepsilon_0\varepsilon_{\pi}}x\right)\mathrm{d}x \quad , \tag{10}$$

where V_{c} and V_{a} are the voltages on both sides of the field control layer and the absorption layer, respectively. If E_{M} reaches the maximum value E_{br} during the avalanche multiplication breakdown, the voltage applied across the device at this time is the avalanche breakdown voltage $V_{\text{br-apd}}$.

2.3 Quantum efficiency and photoresponsivity

Quantum efficiency QE is the number of electron-hole pairs generated inside a semiconductor by a single incident photon[25], which is defined as:

$$QE=\frac{I_{\mathrm{ph}}/q}{P_{\mathrm{opt}}/hv} \quad , \tag{11}$$

where I_{ph} is the photocurrent, P_{opt} is the incident light power, hv is the single-photon energy, and q is the charge of the electron. Assuming that all the carriers generated by the incident illumination of Si-APD under the action of working bias enter the depletion region, the quantum efficiency QE relation can be expressed as:

$$QE=\varphi(1-R)[1-\exp(-\alpha W_{\mathrm{D}})] \quad , \tag{12}$$

where φ is the probability that a single photon absorbed by the material excites a hole-electron pair; R is the reflectivity of the silicon surface, α is the light absorption coefficient of the material, and the relation of R and α on the wavelength is shown in Fig.3 (color online); W_{D} is the depletion layer thickness. Equation (12) shows that the excitation probability φ of photogenerated carriers is fixed, and under the action of incident light of a certain wavelength, the quantum efficiency of APD is mainly affected by the surface reflectivity R and the thickness of the depletion layer W_{D}. For the convenience of calculation, assuming that φ=100%, and all the excited hole-electron pairs can enter the depletion layer, the relation between the quantum efficiency of Si-APD blue light band and the thickness of the depletion layer is calculated by formula (12). The results are shown in Fig.4 (color online), that is, when the depletion layer thicknesses W_{D} are 1.0 μm, 2.0 μm, 3.0 μm, 4.0 μm and 5.0 μm, the corresponding peak quantum efficiencies QE_{peak} are about 55.03%, 58.23%, 59.83%, 60.99% and 61.72%, and the corresponding incident wavelengths λ_{peak} are

0.43 μm, 0.47 μm, 0.49 μm, 0.51 μm and 0.52 μm, respectively.

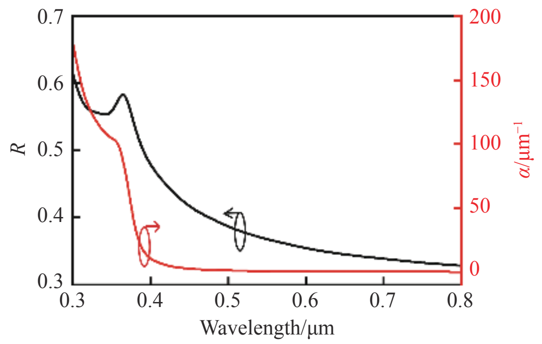

Fig. 3 The surface reflectance and absorption coefficient of the silicon vary with different incident wavelengthes

图 3 硅表面反射率及吸收系数随入射波长的变化情况

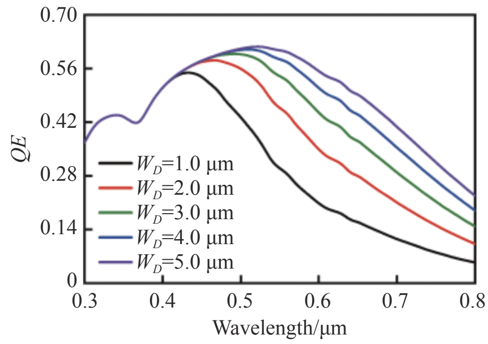

Fig. 4 The relationship between quantum efficient and incident wavelength under different depletion layer thicknesses

图 4 不同入射波长的量子效率与耗尽层厚度的关系

The above calculation curve results show the variation of quantum efficiency with incident wavelength under different depletion layer thickness W_D. It can be seen from the figure that the quantum efficiency increases with the increase of the depletion layer thickness W_D. The analysis shows that with the increase of the incident wavelength, the corresponding absorption coefficient α decreases. The increase in the thickness of the depletion layer can improve the light absorption rate of Si-APD, and correspondingly increase the number of photogenerated electron-hole pairs in the depletion layer. The peak quantum efficiency QE_{peak} red-shifts with the increase of the corresponding incident wavelength and the thickness of the depletion layer. It can be found from the curve in the figure that under the excitation of a specific incident wavelength, the QE peak of the Si-APD quantum efficiency does not increase with the increase of the thickness of the depletion layer. This is because the light absorption of the depletion layer to the incident wavelength is saturated, making the number of photogenerated carriers constant, for example, when the depletion layer thickness $W_D \geqslant 2.0$ μm, the quantum efficiency at the incident wavelength $\lambda=0.45$ μm is fixed at $QE=57.58\%$.

The photoresponsivity SR is a measure of the photoelectric conversion capability of the photodetector on the macroscopic scale, which is defined as the ratio of the photocurrent I_{ph} to the incident optical power P_{opt}, and the expression is $SR=I_{ph}/P_{opt}$. The relationship between optical responsivity and quantum efficiency is[26]:

$$SR = M\frac{\lambda}{1.24}QE \quad , \qquad (13)$$

where M is the gain coefficient. According to the quantum efficiency QE defined by Eq. (12), the above equation can be rewritten as:

$$SR = M\varphi(1-R)[1-\exp(-\alpha W_D)]\frac{\lambda}{1.24} \quad . \qquad (14)$$

Assuming that the gain coefficient $M=1$ and $\varphi=100\%$, the relationship between the optical responsivity SR in the visible light band and the thickness W_D of the depletion layer is calculated according to Eq. (14), as shown in Fig.5 (color online).

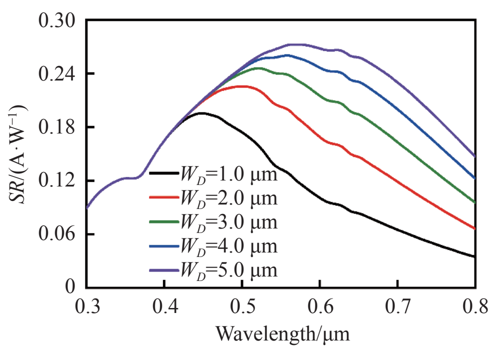

Fig. 5 The relationship between spectral response and incident wavelength under different depletion layer thicknesses

图 5 在不同耗尽层厚度下，光响应度与入射波长的关系

The curves in Fig.5 show that when the depletion layer thickness W_D are 1.0 μm, 2.0 μm, 3.0 μm, 4.0 μm or 5.0 μm, the corresponding peak photoresponsivity SR_{peak} are about 0.196 A·W^{-1}, 0.226 A·W^{-1}, 0.246 A·W^{-1}, 0.261 A·W^{-1}, or 0.272 A·W^{-1}, and the corresponding incident wavelength λ are 0.44 μm, 0.50 μm, 0.52 μm, 0.56 μm, or 0.57 μm, respectively, which are consistent with the incident wavelength corresponding to the peak quantum efficiency.

2.4 Effect of multiplication layer parameters on gain

The photocurrent gain is the most important characteristic of APD, and its underlying physical mechanism is the impact ionization effect of carriers, which is usually expressed by a multiplication factor. Assuming that the avalanche effect only occurs in the multiplication layer, the multiplication factor $M_{(x)}$[27] defined by Eq. (15) shows that the avalanche multiplication is mainly depended on the width of the depletion layer, the electric field strength, the collision ionization coefficient of carriers, etc. In the case of electron-induced avalanches, the multiplication factor $M_{(x)}$ is:

$$M_{(x)} = \frac{1}{1-\int_0^{W_m}\alpha(x)\exp\left(-\int_x^{W_m}[\alpha(x')-\beta(x')]\,\mathrm{d}x'\right)\mathrm{d}x}, \quad (15)$$

where $\alpha(x)$ and $\beta(x)$ are the collisional ionization coefficients of electrons and holes, respectively, and W_m is the thickness of the multiplication region. Chynoweths describes the effect of electric field strength E on the collisional ionization of carriers as[28]:

$$\begin{cases}\alpha(x) = a_n \exp\left[-\left(\dfrac{b_n}{E(x)}\right)\right] \\ \beta(x) = a_p \exp\left[-\left(\dfrac{b_p}{E(x)}\right)\right]\end{cases}, \quad (16)$$

where a_n, b_n, a_p and b_p are the experimental parameters of the collision ionization rate of electrons and holes, respectively, and $E(x)$ is the electric field strength in the multiplication region, which is a function of the distance x. The numerical calculation in this paper adopts Lee's experimental fitting coefficients[29]: a_n=3.8×10^6 cm^{-1}, b_n=1.75×10^6 V·cm^{-1}; a_p=2.25×10^6 cm^{-1}, b_p=3.26×10^6 V·cm^{-1}.

Consider the relationship among the thickness of the multiplication layer in the PN junction, the applied bias voltage V_m on both sides of the multiplication layer, and the multiplication coefficient M under a certain doping concentration. Assuming that the doping concentration of the N-type substrate is N_D=1.0×10^{19} cm^{-3}, and the doping concentration of the P-type multiplication layer is N_A=1.0×10^{16} cm^{-3}, combined with Eqs. (1), (2), and (16), in order to simplify the calculation, perform the third-order Taylor expansion of $\alpha(x)$ and $\beta(x)$, and substitute them into Eq. (15) to calculate the relationship between the applied bias voltage V_m of the multiplication layer and the multiplication coefficient M, the result is shown in Fig.6 (color online).

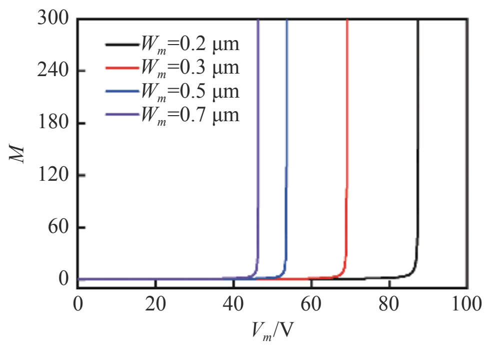

Fig. 6 The relationship between the thickness of multiplication layer and multiplication factor M

图 6 倍增层厚度与倍增系数 M 的关系

The curves in the above figure show that M increases sharply when the applied bias voltage V_m on both sides of the multiplication layer increases to a specific value, and Equation (15) shows that V_m is close to or equal to the voltage $V_{br\text{-}m}$ on both sides of the multiplication layer at the time of avalanche breakdown. Therefore, in order to obtain a higher gain for the APD, the applied bias voltage V_{apd} acting on the device needs to approximate the avalanche breakdown voltage $V_{br\text{-}apd}$ of the device. The curves in the figure shows that as the thickness of the multiplication layer increases, the voltage to obtain the same multiplication factor decreases. That is, at small multiplication layer thickness, the voltage needs to be increased so that the carriers have a higher ionization rate in order to obtain a higher gain. However, the increase of the thickness of the multiplication layer is affected by the doping concentration and the applied bias voltage at both ends of the PN junction, and the selection of the thickness is also based on the electric field distribution, which is related to the doping concentration, so the thickness of the multiplication layer needs to be comprehensively considered with its doping concentration.

For silicon, the carrier energy is completely lost in the collisional ionization only when the electron energy is $E_{ele} \geqslant 6.5$ eV[30]. From the perspective of energy, it is assumed that the collision ionization effect occurs only in the multiplier layer, the influence of field control layer on electron energy is not considered, and the hole electron recombination mechanism and scattering energy loss are ignored. It can be seen from formula (4), that let the carrier obtain energy under the action of the electric field of the multiplication layer ΔE is:

$$\Delta E = e\int_0^{W_m}\left(E_M - \frac{qN_p}{\varepsilon_0\varepsilon_p}x\right)dx \quad . \qquad (17)$$

For the convenience of calculation, the critical breakdown electric field intensity E_M is substituted into the above formula ΔE, and we have:

$$\Delta E = e\int_0^{W_m}\left(\frac{4\times10^5}{1-(1/3)\log_{10}(N/10^{16})} - \frac{qN_p}{\varepsilon_0\varepsilon_p}x\right)dx = e\left(\frac{4\times10^5}{1-(1/3)\log_{10}(N/10^{16})}W_m - \frac{qN_p}{2\varepsilon_0\varepsilon_p}W_m^2\right) \quad . \qquad (18)$$

The doping concentration of the substrate is set to $N_{n++}=1.0\times10^{19}$ cm^{-3}, the doping concentration of the multiplication layer N_p is 1.0×10^{15}~1.0×10^{17} cm^{-3}, and the PN junction is set as a unilateral mutation junction. According to Eq. (18), the numerical relationship between the doping concentration and the carrier energy ΔE under different multiplication layer thicknesses was calculated, and the results are shown in Fig. 7 (color online). When the thickness of the fixed multiplication layer is W_m=0.5 μm, the curves in the figure show that when the doping concentrations N_p is 1.2×10^{16} cm^{-3}, 1.8×10^{16} cm^{-3} or 2.4×10^{16} cm^{-3}, the energy ΔE is 18.22 eV, 18.39 eV or 18.26 eV, respectively. Therefore, when the doping concentration of the multiplication layer is 1.8×10^{16} cm^{-3}, the carriers obtain a higher energy ΔE=18.39 eV in the multiplication layer, which can theoretically generate a higher gain coefficient M.

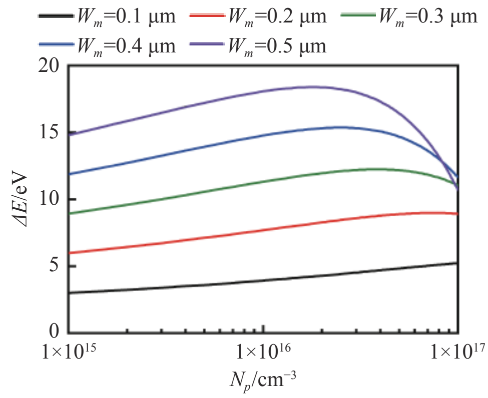

Fig. 7 Relationship between carrier energy ΔE and multiplication layer doping concentration

图 7 载流子获得能量 ΔE 与倍增层掺杂浓度的关系

2.5 Influence of field control layer

The doping concentration (N_{p+}) and the thickness (W_c) of the field control layer are important for adjusting the electric field intensity between the multiplication layer and the absorption layer. The field control layer is located between the absorption layer and the multiplication layer, and reduces the tunneling probability of the device by reducing the electric field strength of the absorption layer. However, the thickness of the field control layer should not be too large. The reasons are as follows: when the applied bias voltage and the doping concentration of the field control layer are fixed, increasing the thickness of the field control layer will reduce the electric field strength of the absorption layer, and affect the drift velocity of photogenerated carriers in the absorption layer; if the thickness is too small, it will increase the electric field strength of the absorption layer, induce carrier ionization, and increase unnecessary noise current. According to Eq. (5), under the condition of ensuring the carrier saturation drift velocity, the appropriate doping concentration and thickness is beneficial to the modulation and transition of the electric field between the multiplication layer and the absorption layer. In general, compared with multiplication. a smaller thickness and a higher doping concentration should be chosen to ensure the least effect on the multiplication layer variation.

2.6 Design of absorption layer

Due to the absorption characteristics of Si material itself[31], the blue light band in the wavelength range of 0.4 ~ 0.5 μm has a high absorption coefficient (as shown in Fig.3), which leads to a shallow penetration depth of light in the blue light band, about 0.098~0.82 μm in silicon. In order to fully absorb the blue light by the absorption layer, the thickness of the absorption layer W_a=1.3 μm is selected in combination with the relationship between the quantum efficiency and the thickness of the depletion layer shown in Fig. 4. In silicon, when the electric field strength E>1.0×10^4 V·cm^{-1}, the velocity of electrons tend to the saturation drift velocity, that is, v_s(Si)≈10^7 cm·s^{-1}. In order to keep the high bandwidth of the device, the carriers should move at the saturation velocity in the device. When the doping concentration and thickness of the multiplication layer and the field control layer are fixed (W_m=0.5 μm, N_p=1.8×10^{16} cm^{-3}; W_c=0.2 μm, N_{p+}=8.0×10^{16} cm^{-3}), and the mutation PN junction is close to breakdown, the field strength distribution of the absorption layer under different doping concentrations is drawn according to Eq. (6), as shown in Fig. 8 (color online). It can be seen from the figure that the field strength of the absorption layer gradually decreases with the increase of the doping concentration. When the doping concentration of the absorption layer is N_π=1.0×10^{16} cm^{-3} and 5.0×10^{15} cm^{-3}, the field strength has been exhausted before reaching the surface non-depletion region, and at this time, the blue-light excited carriers enter the absorption layer and are dominated by diffusion motion, which increases the carrier transit time and reduces the device bandwidth. When N_π *is* 1.0×10^{14} cm^{-3}, 5.0×10^{14} cm^{-3} or 1.0×10^{15} cm^{-3}, respectively, the edge field strength of the absorption layer is E>10^4 V·cm^{-1}, the device is in the pull-through state, and the carriers drift at the saturation velocity in the whole device. Therefore, the doping concentration and thickness of the absorption layer should be selected so that the absorption layer have a good electric field distribution and the carriers move in this layer at a saturated drift velocity, and that the red and green light has a certain absorption rate at the same time.

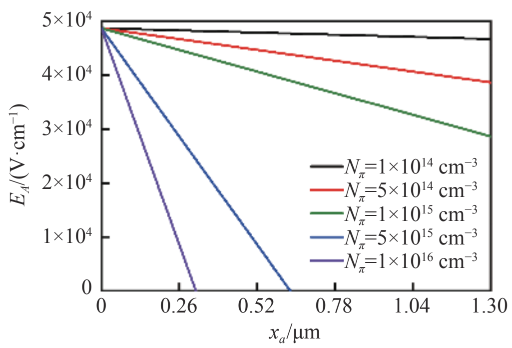

Fig. 8 Field intensity distribution of the absorption layer under different doping concentrations

图 8 不同吸收层掺杂浓度下吸收层的场强分布

2.7 Si-APD initial structural parameters

Assuming that the layers are uniformly doped, the incident light is absorbed only in the absorption layer, and under reverse bias voltage, the avalanche effect occurs only in the multiplication layer. Based on the relationship among the gain coefficient, the applied bias voltage and the thickness of the multiplication layer, the relationship among the quantum efficiency, the photoresponsivity and the thickness of the depletion layer, the selected parameters of each layer are shown in Table 1, where W_s, W_a, W_c,

Tab. 1 Parameters of Si-APD layers

表 1 Si-APD 各层参数

Parameter	Thickness/μm	Doping type	Impurity concentration/(cm^{-3})
W_s	0.06	p++	N_{p++}= 1.0×10^{18}
W_a	1.30	p-	N_π = 1.0×10^{15}
W_c	0.20	p+	N_{p+} = 8.0×10^{16}
W_m	0.50	p	N_p = 1.8×10^{16}
W_{sub}	20.00	n++	N_{n++} = 1.0×10^{19}

W_m and W_{sub} are the thicknesses of the surface non-depletion layer, absorption layer, field control layer, multiplication layer and substrate, respectively.

3 Si-APD numerical calculation

The basic equations of semiconductor device operation include electrostatic equation, current density equation and continuity equation. The generation and recombination mechanism of carriers is the key to the performance of semiconductor photodetectors. In the two-dimensional simulation of the device characteristics of Si-APD, the diameter of the photosensitive surface of the Si-APD used in the calculation is 10 μm. In order to improve the accuracy of the calculation results, physical models such as Selberherr's ionization[32, 33], Shockley-Read-Hall recombination[34, 35] and carrier mobility[36-38] are used in the calculation.

3.1 The relationship between the field strength distribution of Si-APD and the applied bias voltage

According to the parameters in Table 1, when the V_{apd} in the device is 0 V, 0.5 $V_{br\text{-}apd}$, 0.7 $V_{br\text{-}apd}$ or $V_{br\text{-}apd}$ respectively (the corresponding V_{apd} is 0 V, 17.1 V, 23.9 V, 34.2 V), the field strength distribution inside the Si-APD as shown in Fig.9 (color online). It can be seen from the figure that the electric field strength inside the Si-APD increases with the increase of the bias voltage V_{apd} applied to the device. When V_{apd} is small, the device is in a non-

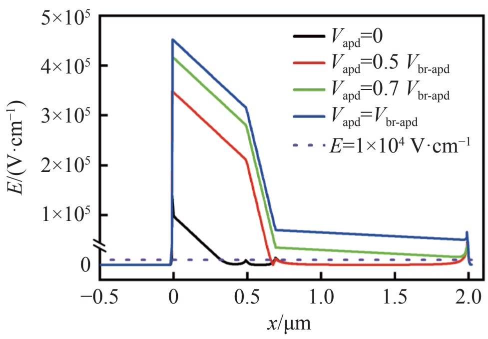

Fig. 9　The field strength distribution of Si-APD under different applied bias voltages

图 9　不同外加偏压下 Si-APD 的场强分布

pull-through state, and the carriers begin to diffuse in the device. With the increase of the applied bias voltage, the device is pulled through as a whole, at this time, the carriers are dominated by drift motion. As the applied bias voltage is continuously increased, the carriers will eventually move in the device at the saturation drift velocity.

3.2 Further optimization of the thickness of non-depletion layer on the surface

Generally, the surface of the semiconductor photodetector has a certain thickness of the surface heavily doped non-depletion layer (also act as an electrode layer), and the penetration depth of light in the blue light band in silicon is relatively small. When light passes through the non-depleted layer at the top of the device, most of the blue light energy is absorbed by this layer to generate hole-electron pairs, so it is necessary to optimize the thickness of the surface non-depleted layer. On the basis of the parameters in Table 1, the impurity concentration of the surface layer and the structural parameters of other doped layers are fixed, the incident light is vertically irradiated on the surface layer of the detector, and the spectral response curves of different surface non-depleted layer thicknesses are obtained when $R\neq0$, which are shown in Fig.10 (color online).

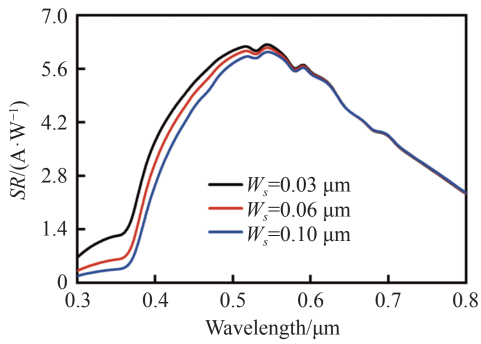

Fig. 10　Effect of thickness of surface layers of Si-APD on spectral responsivity

图 10　不同表面层厚度 Si-APD 的光谱响应曲线

The curve in the figure shows the spectral responsivity under the applied bias voltage of 0.95 $V_{br\text{-}apd}$ ($M\approx26$) when the thickness of the surface non-depletion layer is W_s=0.03 μm, 0.06 μm and 0.10 μm. When W_s=0.03 μm, the photoresponsivity of the blue band SR is 3.71~6.08 A·W^{-1}; when W_s=0.06 μm, the photoresponsivity SR of the blue band is 3.15~5.94 A·W^{-1}; when W_s = 0.10 μm, the photoresponsivity SR in the blue band is 2.57~5.75 A·W^{-1}, indicating that the smaller the thickness of the surface non-depletion layer is, the smaller the inhibitory effect on the photoresponsivity of blue light will be. It is also found from the curve that the change of W_s has little effect on the optical responsivity of the device in the long wavelength band. The analysis shows that according to the transmission characteristics of light in the medium, the light absorption loss A_s of the incident light in the surface non-depletion layer with a thickness of W_s is

$$A_s = (1-R)[1-\exp(-\alpha W_s)] \quad , \tag{19}$$

where R is the surface reflectance, and α is the light absorption coefficient of Si. The drift current density formed by photogenerated carriers in the depletion region of width W_D is:

$$J_{ph} = q\frac{(1-R)\exp(-\alpha W_s)P_{opt}}{A\cdot h\upsilon}\cdot[1-\exp(-\alpha W_D)]. \tag{20}$$

For the fixed incident optical power P_{opt} in the visible light band, the first half of Eq. (20) represents the number of photons that penetrate to the edge of the depletion layer of the detector at a specific wavelength, and the second half represents the absorption rate of the incident photons by the depletion layer with a thickness of W_D. Ignoring the recombination mechanism of carriers, set the quantum efficiency QE=100% in the depletion region. According to the material characteristics of Si, the intensity of long-band incident light absorbed by the material is small, so the light absorption loss generated by the surface non-depletion layer has little effect on the light energy transmitted to the depletion layer. Therefore, the long wave band light response is basically stable in the process of adjusting W_s. However, on the short-wave side, the thickness of the surface non-depletion layer has a great influence on the optical responsivity.

3.3 Effect of doping concentration of multiplication layer on optical responsivity

According to the calculation results in Fig.10 and the calculation results of the surface non-depletion layer thickness above, take the surface non-depletion layer thickness W_s=0.03 μm, the surface reflectivity R≠0, and other parameters are based on the data in Table 1 to obtain that when V_{apd}=0.95 $V_{br\text{-}apd}$, the photoresponsivity of Si-APD in the visible light band is shown in the red curve in Fig.11 (color online), and the corresponding photoresponsivity SR in the blue light band is divided into 3.72~6.08 A·W^{-1}.

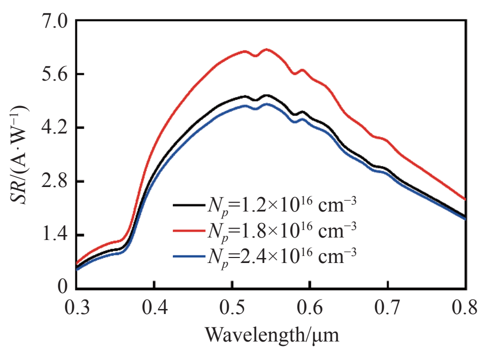

Fig. 11 Effect of doping concentration of multiplication layer on spectral responsivity

图 11 倍增层掺杂浓度对光响应度的影响

For comparison, when other parameters remain unchanged, the doping concentrations of the multiplication layer N_P are calculated as 1.2×10^{16} cm^{-3}, 2.4×10^{16} cm^{-3} (the corresponding breakdown voltage $V_{br\text{-}apd}$ is 39.2 V and 30 V respectively). The photoresponsivity at V_{apd}=0.95 $V_{br\text{-}apd}$ are shown in the blue and black lines in Fig.11 (color online). The corresponding photoresponsivity in the blue light band SR are divided into 3.02~4.93 A·W^{-1} and 2.83~4.68 A·W^{-1}. In both cases, the photoresponsivity is lower than the SR value for N_p=1.8×10^{16} cm^{-3} doping indicated by the red line.

This phenomenon can be attributed to the fact that at this doping concentration, the carriers can gain higher energy in the multiplication layer (as shown in Fig.7), resulting in a greater photocurrent gain. Based on the above results, the basic epitaxial structure parameters of the Si photodetector were finally determined as shown in Table 2.

Tab. 2　Parameters of Si-APD layers

表 2　Si-APD 各层参数

Parameter	Thickness/μm	Doping type	Impurity concentration/ (cm^{-3})
W_s	0.03	p++	$N_{p++}=1.0\times10^{18}$
W_a	1.30	p-	$N_\pi=1.0\times10^{15}$
W_c	0.20	p+	$N_{p+}=8.0\times10^{16}$
W_m	0.50	p	$N_p=1.8\times10^{16}$
W_{sub}	20.00	n++	$N_{n++}=1.0\times10^{19}$

3.4　I-V characteristics of Si-APD dark current

Assuming that each layer is uniformly doped, the I-V relationship characteristics of the Si-APD in the dark environment can reflect the electrical parameters such as the avalanche breakdown voltage $V_{br\text{-}apd}$ and the current gain coefficient M of the device. The I-V characteristic curves are calculated qualitatively according to the parameters in Table 2 and the current density equation defined in Equation (21). The current density magnitude is mainly influenced by the carrier transport behavior and is expressed in the numerical relationship as the sum of electron current density and hole current density, i.e.:

$$\begin{cases} J_n = qn\mu_n E + qD_n\nabla n \\ J_p = qp\mu_p E - qD_p\nabla p \\ J_{cond} = J_n + J_p \end{cases} , \qquad (21)$$

where J_n is the electron current density, J_p is the hole current density, J_{cond} is the conduction current density, μ_n is the electron mobility, μ_p is the hole mobility, D_n is the electron diffusion coefficient, D_p is the hole diffusion coefficient, ∇n and ∇p are the excess carrier concentration gradients. The curve in Fig.12 (color online) shows the calculated reverse current as a function of the applied bias voltage V_{apd}. It can be seen from the figure that the magnitude of the current increases with the increase of V_{apd}, but the change trend of the current is different. According to different current formation mechanisms, it is summarized as parts (i)-(iv) in Fig.12.

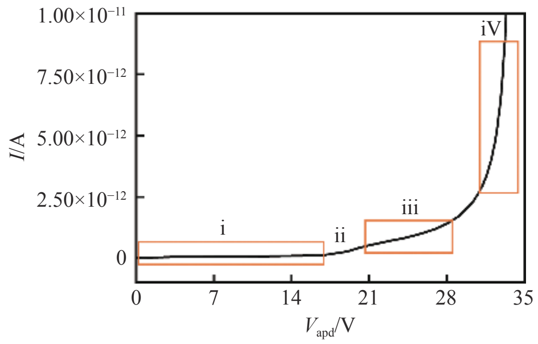

Fig. 12　The dark current I-V curve of Si-APD

图 12　Si-APD 暗电流的 I-V 曲线

The dark current density of avalanche photodiode includes[39] recombination current density J_r, minority carrier diffusion current density J_{diff}, carrier drift current density J_{dr} of depletion layer and avalanche current density J_m. The recombination current density is expressed as $J_r=qn_iW_D/2\tau_D$. $\tau_D=1/R_{ec}\cdot N$ is the carrier lifetime, $R_{ec}\approx10^{-15}$ cm^3s^{-1} is the indirect band gap semiconductor recombination coefficient[27], and N is the doping concentration. $J_{diff}=(qD_pn_i^2/L_pN_D)+(qD_nn_i^2/L_nN_A)$, $D_p=kT\mu_p/q$ and $D_n=kT\mu_n/q$ are the diffusion coefficient of hole and electron respectively, L_p and L_n are the diffusion length of hole and electron respectively. When T=300 K, kT/q=0.0259 V, D_p=12.95 $cm^2\cdot s^{-1}$, D_n=37.56 $cm^2\cdot s^{-1}$. For simple calculation, combined with the doping concentration of π absorption layer, p+ type field control layer and p type multiplication layer in the APD structure designed above, the three regions are regarded as p type silicon materials with doping concentration $\overline{N_A}$ and carrier life $\overline{\tau_{sc}}$:

$$\overline{N_A} = \frac{N_p + N_{p+} + N_\pi}{3} = 3.3\times10^{16}\ cm^{-3} , \qquad (22)$$

$$\overline{\tau_{sc}} = \frac{\tau_{sc(p)} + \tau_{sc(p^+)} + \tau_{sc(\pi)}}{3} = 0.356\ s , \qquad (23)$$

where $\tau_{sc(p)}$, $\tau_{sc(p+)}$ and $\tau_{sc(\pi)}$ are the carrier lifetimes of the multiplication layer, the field control layer and the absorption layer, respectively.

When the applied bias voltage V_{apd} is small, the Si-APD current is dominated by the diffusion and recombination currents. Substituting the above data into equation (24) to calculate the diffusion and recombination currents of the device, the results correspond to part (i) in Fig.12.

$$I_{(i)} = \int_0^{W_D} (J_r + J_{\text{diff}})\,dx \quad . \qquad (24)$$

When increasing the applied bias voltage V_{apd}, the number of carriers subjected to the internal electric field increases and the drift current accounts for the major part of the current. According to equation (21), the drift current density of the device is expressed as $J_{\text{dr}}=qn\mu_n E+qp\mu_p E$, where E is the electric field strength of the depletion layer defined by equations (4) to (7). Substituting the calculated J_{dr} into the following equation, the result corresponds to part (ii) in Fig.12.

$$I_{(ii)} = \int_0^{W_D} (qn\mu_n E + qp\mu_p E)\,dx \quad . \qquad (25)$$

If the applied bias voltage V_{apd} continues to increase, the carriers collide and ionize under the action of strong electric field. The high-energy initial carriers collide with the internal lattice to produce secondary carriers, and then continue to collide with the lattice to produce new carriers to form avalanche current density $J_m=\alpha_n J_n+\alpha_p J_p$, J_n and J_p are electron and hole current densities, α_n, α_p are the ionization coefficient of electrons and holes, respectively. The collision effect continues under the working bias voltage and the number of carriers is doubled. Assuming that the avalanche effect only occurs in the multiplication layer, the avalanche dark current I_d generated in the multiplication layer with a thickness of W_m can be expressed as:

$$I_d = \int_0^{W_m} \left(\alpha_n J_n + \alpha_p J_p\right) dx \quad . \qquad (26)$$

As shown in part (iii) of Fig.12.

Generally, the gain coefficient M of the device can be obtained from the following empirical relation

$$M = \frac{I_d}{I_{d_0}} = \frac{1}{1-\left(\frac{V_{\text{apd}}}{V_{\text{br-apd}}}\right)^n} \quad , \qquad (27)$$

where I_d is the dark current generated based on the impact ionization of the carriers, I_{d0} is the initial dark current, the constant n is affected by the device structure, doping distribution and other factors, usually the n of the Si material is 1.5−4.0. When the applied bias voltage V_{apd} is close to the avalanche breakdown voltage $V_{\text{br-apd}}$, the current will increase with the sharp increase of the multiplication factor M, as shown in the area (iv) in Fig.12.

The dark current I-V curve in Fig.12 shows that when the APD device is at a low applied bias voltage, the diffusion current accounts for most of the total current; after that, the internal electric field strength will increase with the increase of V_{apd}, and the width of the depletion region will increase too. More carriers enter the depletion region to form a drift current under the action of the electric field, which becomes the main part of the total current; when V_{apd} continues to increase, due to the impact ionization of carriers, there will be a current gain phenomenon, but the effect is not obvious; if V_{apd} is close to the device avalanche breakdown voltage $V_{\text{br-apd}}$, and there will be a sharp increase in current.

By comparing the variation trend of current with voltage in parts (iii) and (iv), it can be found that APD can produce a higher current gain M when the bias voltage is higher than the avalanche breakdown voltage. According to the analysis, the ionization rate of the carrier is an important indicator to measure the avalanche multiplication effect, which is closely related to the electric field strength associated with the device bias voltage[40], and the ionization rate increases with the increase of the bias voltage. Taking the carriers in the multiplication layer as an example, the impact ionization rate distributions of electrons and holes under different bias voltages are calculated according to Equation (16), *Lee*'s carrier ionization parameter and the electric field distribution of Equation (4), Figs. 13 (a) and 13(b) (color online) clearly show that the collision ionization coefficient increases with the increase of the voltage V_m on both sides of the multiplication layer, so when V_{apd} approaches $V_{\text{br-apd}}$, there will be a high current gain, and the electron gain is dominant.

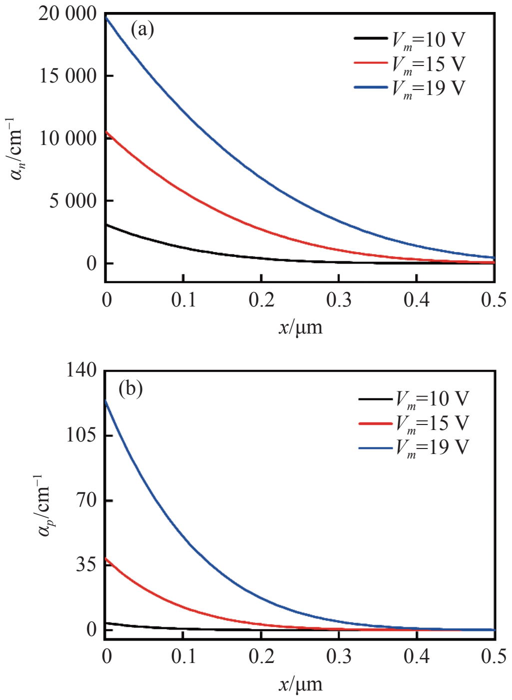

Fig. 13　(a) Electron ionization coefficients in the multiplication layer under different bias voltages; (b) hole ionization coefficients in the multiplication layer under different bias voltages.

图 13　(a) 不同倍增层偏压下倍增层内电子离化系数; (b) 不同倍增层偏压下倍增层内空穴离化系数

4　Conclusion

In order to meet the urgent demand for blue light high response photodetectors in optical communication systems, a SACM type Si-APD structure with interchangeable positions of absorption layer and multiplication layer is designed and the relationship between multiplication layer thickness and device gain, absorption layer doping concentration and absorption layer field strength distribution, external bias and internal field strength distribution, surface non-depletion layer thickness and spectral response, and multiplication layer concentration and spectral response are studied. After comprehensive consideration, the structural parameters of the device are selected as follows: the thickness of the surface non-depletion layer is 0.03 μm, the doping concentration is 1.0×10^{18} cm^{-3}; the thickness of absorption layer is 1.3 μm, the doping concentration is 1.0×10^{15} cm^{-3}; the thickness of field control layer is 0.2 μm, the doping concentration is 8.0×10^{16} cm^{-3}; the thickness of multiplication layer is 0.5 μm, the doping concentration is 1.8×10^{16} cm^{-3}. The device has a low breakdown voltage $V_{br\text{-}apd}$=34.2 V. When V_{apd}=0.95 $V_{br\text{-}apd}$, it has a high optical responsivity of 3.72 ~ 6.08 A·W^{-1} in the blue band. The results of this paper have a certain reference value for the preparation of actual devices.

——中文对照版——

1　引　言

随着短波长可见光光源(如蓝光 LED、蓝光半导体激光器等)的发展和广泛应用,短波长可见光高效探测技术的应用越来越广泛。尤其是可见光通信技术[1]、生物医学工程、水下光通信[2]等领域的快速发展,迫切需要具有高带宽、高增益、宽光谱、高光响应的可见光探测器[3]。白光 LED 是可见光通信的重要光源[4],目前常用的白光 LED 主要有荧光型白光 LED(通过蓝光 LED 激发荧光粉混合形成白光[5])、红蓝绿型白光 LED(RGB-LED)[6],上述两种白光 LED,蓝光都是主要的工作波段,因此具有蓝光高响应的光电探测器对进一步促进照明通讯一体化的发展应用具有重要意义[7]。目前常用的光电探测器主要为:PIN 光电二极管(PIN-PD)、光电倍增管(Photo Multiplier Tube, PMT)和雪崩光电二极管(Avalanche Photodiode, APD)。然而,PIN 光响应度低、探测距离短,对光源功率要求高,限制了其在可见光通信中的进一步应用[8]。光电倍增管(PMT)可以探测短波长,然而电压高、对磁场敏感等缺点限制了其在可见光通信方面的应用[9]。雪崩光电探测器(APD)是一种具有较高的内部增益和高光响应度的半导体探测器[10],并且没有 PMT 的上述缺点,在可见光探测器的研究中引起了广泛关注。

硅(Si)对于 380 ~ 1100 nm 波段的入射光均

有吸收能力，是制备宽光谱探测器的良好材料[11]，且 Si 半导体器件制备工艺成熟[12]，同时硅材料中电子与空穴的碰撞电离率比值高、隧道电流低[13]，使得硅基雪崩光电二极管(Si -APD)具有增益高，噪声低，稳定性好等优点。然而由于蓝光在硅中的高吸收系数特性使得蓝光在硅中的透入深度较低，大部分的光生载流子位于浅表层，易导致部分载流子在浅表面复合，进入吸收层的光生载流子数量较少，降低了蓝光波段的光电转换效率，这给蓝光高响应度的 Si-APD 的器件设计和制备带来较大难度。为了提高硅对蓝光的探测效率，改善 Si-APD 在蓝光波段的性能，研究人员进行了相关的研究：2010 年，Excelitas 公司的 Catherine M. Pepin 等人通过在外延片上“埋结”，制备了一种紫外增强型 Si 基 APD，该器件的雪崩击穿电压为 400 V，在 430 nm 波长处的响应度为 39 A/W (M=150)[14]。2015 年，Othman 等人通过 CMOS 工艺将 Si 基 APD 高度集成，雪崩击穿电压为 10 V，在 405 nm 波长处的增益为 100[15]。同年，王旭东等人基于吸收场控倍增分离 (SACM) 型 Si-APD(n-p-p^+-p-p^+型掺杂结构，光从 N 型层表面入射)优化了器件结构参数，同时在器件表面设计了折射率高低交替分布的增透膜结构，优化后器件的峰值响应波长为 406 nm，雪崩击穿电压为 105.9 V，峰值波长处的光响应度为 250 A/W [16]。2015 年，霍林章等人提出了一种深槽隔离结构的 SiPM 探测器，提高了在蓝紫光区(360~420 nm)的探测效率，该器件的击穿电压约为 90V[17]。2019 年，鲁欢欢等人设计了一种 SAM 型 Si-APD，该器件的倍增层更靠近光敏层，能够有效降低光生载流子的复合损耗，该器件的击穿电压约为 50 V，450 nm 处的光响应度为 31.1 A/W[18]。上述研究改善了所设计的 Si-APD 器件的蓝光探测效率。随着需求的日益增长，有必要对 Si-APD 器件作进一步研究，以提高其蓝光探测性能。传统的 Si-APD 器件雪崩击穿电压 V_{br} 较高(150~500 V)，而高的雪崩击穿电压使得器件功率变大，稳定性变差。为获得在蓝光波段的硅基 APD 器件的高蓝光响应度和较低的雪崩击穿电压，本文在传统的 Si-APD 结构基础上，根据光激发载流子的输运特征，优化设计了一种吸收层与雪崩层位置互换的结构，并对结构在蓝光波段进行了优化。对器件倍增层的掺杂浓度及厚度与雪崩击穿电压和光谱响应度的关系进行了研究。本文为设计与制备实际高蓝光响应度硅基雪崩光电探测器芯片提供参考。

2 器件外延结构设计

2.1 SACM 型 Si-APD

根据对 Si 吸收可见光特性(本文所使用的 Si 材料参数来自于 Schinke 等人的实验测量值[19])和 Si 雪崩光探测器工作原理的分析，本文采用一种 SACM 型器件结构，即：吸收层和倍增层分离，并在二者之间加入场控层，将倍增层后置[20-21]。SACM 型 Si-APD 基本外延结构如图 1(彩图见期刊电子版)所示。器件自上而下分别为 p^{++}型重掺杂表面非耗尽层、π 型吸收层、p^+场控层、p 型倍增层以及 n^{++}型衬底，光从 p^{++}非耗尽层表面入射。吸收层可吸收波长为 0.3~1.1 μm 的入射光，覆盖可见光波段；场控层用于调制器件中倍增层与吸收层的电场，实现吸收层的低电场强度和倍增层的高电场强度良好过渡，在保证光生载流子能输运到雪崩层的前提下，抑制噪声载流子[22]；倍增层用于实现初始光生载流子的数量增益；表面非耗尽层和重掺杂衬底兼具导电电极作用。当外加偏压足够高时，器件将处于拉通状态，即耗尽区从 PN 结直到表面非耗尽层，在保证倍增层的雪崩击穿的同时，也保证吸收层电场足够高，使光生载流子能够达到饱和漂移速度从而运动到倍增层。

2.2 Si-APD 电场分布

PN 结耗尽层的电场分布可以表示为：

$$E(x)=E_{\mathrm{M}}-\frac{qN_{\mathrm{m}}}{\varepsilon_0\varepsilon_{\mathrm{m}}}x\quad, \tag{1}$$

式中，q 为单电荷量，N_{m} 为杂质浓度，ε_{m} 为掺杂材料的相对介电常数，ε_0 为真空介电常数，E_{M} 为 PN 结内最大电场强度，E_{M} 由倍增层两侧的掺杂浓度及外加偏压 V_{m} 决定，表示为，

$$E_{\mathrm{M}}=\left[\frac{2q(V_{\mathrm{m}}+V_{\mathrm{bi}})}{\varepsilon_0\varepsilon_{\mathrm{m}}}\cdot\frac{N_{\mathrm{A}}N_{\mathrm{D}}}{N_{\mathrm{A}}+N_{\mathrm{D}}}\right]^{\frac{1}{2}}\quad, \tag{2}$$

其中 N_{D} 为施主杂质浓度，N_{A} 为受主杂质浓度，V_{bi} 为倍增层的内建电势，V_{m} 为倍增区两侧的电

压，表示为：

$$V_{bi} = \frac{KT}{q} \ln\left(\frac{N_A N_D}{n_i^2}\right) \quad , \tag{3}$$

式中，K 为玻尔兹曼常数，T 为开尔文温度（T=300 K），n_i 为本征载流子浓度（n_i=1.02×10^{10} cm^{-3}[23]）。

根据公式(1)，推导求出图 2(彩图见期刊电子版)中器件各层电场表达式(本文中没有考虑同质结因掺杂浓度不同产生的内建电势)。

当 $0 < x < x_1$ 时，

$$E(x) = E_M - \frac{qN_p}{\varepsilon_0 \varepsilon_p} x \quad , \tag{4}$$

当 $x_1 < x < x_2$ 时，

$$E(x) = E_M - \frac{qN_p}{\varepsilon_0 \varepsilon_p} x_1 - \frac{qN_{p+}}{\varepsilon_0 \varepsilon_{p+}} x \quad , \tag{5}$$

当 $x_2 < x < x_3$ 时，

$$E(x) = E_M - \frac{qN_p}{\varepsilon_0 \varepsilon_p} x_1 - \frac{qN_{p+}}{\varepsilon_0 \varepsilon_{p+}} x_2 - \frac{qN_\pi}{\varepsilon_0 \varepsilon_\pi} x \quad , \tag{6}$$

当 $x_3 < x < x_4$ 时，

$$E(x) = E_M - \frac{qN_p}{\varepsilon_0 \varepsilon_p} x_1 - \frac{qN_{p+}}{\varepsilon_0 \varepsilon_{p+}} x_2 - \frac{qN_\pi}{\varepsilon_0 \varepsilon_\pi} x_3 - \frac{qN_{p++}}{\varepsilon_0 \varepsilon_{p++}} x, \tag{7}$$

式中，N_p、N_{p+}、N_π 和 N_{p++}分别为倍增层、场控层、吸收层和表面非耗尽层的掺杂浓度，通过调整各层掺杂浓度和厚度，可以设计和调整各层中的电场分布及相应的电压；E_m 为图 2 中，$x = 0$ 位置处的电场强度，也为器件中的电场强度最大值；ε_p、ε_{p+}、ε_π 与 ε_{p++}表示倍增层、场控层、吸收层与表面非耗尽层的相对介电常数。掺杂硅的相对介电常数[24] 表达式分别为：

N 型掺杂硅：

$$\varepsilon_{Si}(N_D) = \frac{1.635\times10^{-19} N_D}{1+1.172\times10^{-21} N_D} + 11.688 \quad , \tag{8}$$

P 型掺杂硅：

$$\varepsilon_{Si}(N_A) = \frac{1.5\times10^{-16} N_A}{105.3 - 4.949\,6\times10^{-5} N_A^{1/3} - 3.283\times10^{-18} N_A} + 11.7. \tag{9}$$

如果确定了各层厚度和掺杂浓度，根据公式(4)−(7)定义的器件内部电场分布，图 1 中 Si-APD 器件上的电压 V_{apd} 的表达式为：

$$V_{apd} = V_m + V_c + V_a = \int_0^{x_1} \left(E_M - \frac{qN_p}{\varepsilon_0 \varepsilon_p} x\right) dx + \int_{x_1}^{x_2} \left(E_M - \frac{qN_p}{\varepsilon_0 \varepsilon_p} x_1 - \frac{qN_{p+}}{\varepsilon_0 \varepsilon_{p+}} x\right) dx + \int_{x_2}^{x_3} \left(E_M - \frac{qN_p}{\varepsilon_0 \varepsilon_p} x_1 - \frac{qN_{p+}}{\varepsilon_0 \varepsilon_{p+}} x_2 - \frac{qN_\pi}{\varepsilon_0 \varepsilon_\pi} x\right) dx \quad . \tag{10}$$

V_c 和 V_a 分别为场控层、吸收层两侧的电压。如果 E_M 达到雪崩倍增击穿时的最大值 E_{br}，那么，此时器件两端所加的电压则为雪崩击穿电压 $V_{br\text{-}apd}$。

2.3　量子效率与光响应度

量子效率 QE 为单入射光子在半导体内部产生电子-空穴对的数目[25]，定义式为：

$$QE = \frac{I_{ph}/q}{P_{opt}/h\nu} \quad , \tag{11}$$

式中，I_{ph} 表示光电流，P_{opt} 表示入射光功率，$h\nu$ 为单光子能量，q 为电子的电荷量。假设Si-APD 在工作偏压作用下入射光照产生的载流子全部进入耗尽区，量子效率 QE 关系式可表达为：

$$QE = \varphi(1-R)[1-\exp(-\alpha W_D)] \quad , \tag{12}$$

式中，φ 为被材料吸收的单光子激发空穴-电子对的概率；R 为硅表面反射率，α 为材料的光吸收系数，R、α 对波长的依赖关系如图 3(彩图见期刊电子版)所示；W_D 为耗尽层厚度。式(12)表明，光生载流子的激发概率 φ 固定，在一定波长的入射光作用下，APD 的量子效率主要受表面反射率 R 与耗尽层厚度 W_D 的影响。为计算方便，假设 φ=100%，且激发空穴-电子对都可以进入耗尽层，通过式(12)计算得出 Si-APD 蓝光波段的量子效率与耗尽层厚度的关系，结果如图 4(彩图见期刊电子版)所示。图 4 中曲线展示了耗尽层厚度 W_D 分别为 1.0、2.0、3.0、4.0 与 5.0 μm 时，所对应的峰值量子效率 QE_{peak} 分别为 55.03%、58.23%、59.83%、60.99% 和 61.72%，相应的入射波长 λ_{peak} 分别为 0.43 μm、0.47 μm、0.49 μm、0.51 μm 和 0.52 μm。

图 4 给出了不同耗尽层厚度 W_D 时量子效率随入射波长的变化情况。从图中可以看出：量子效率随耗尽层厚度 W_D 的增加而提高。分析认为，随着入射波长的增加，相应的吸收系数 α 减

小，而耗尽层厚度增大可提高 Si-APD 的光吸收率，相应地增加耗尽层内光生电子-空穴对的数量，峰值量子效率 QE_{peak} 随相应入射波长、耗尽层厚度的增加而红移。通过图中曲线可以发现，Si-APD 在特定入射波长的激励下，量子效率 QE 峰值不随耗尽层厚度的增加而提高，这是由于耗尽层对该入射波长的光吸收饱和，使光生载流子数量恒定，因此出现量子效率稳定现象，例如当耗尽层厚度 $W_D \geqslant 2.0$ μm 时，入射波长 λ=0.45 μm 的量子效率固定为 QE=57.58%。

光响应度 SR 是衡量光电探测器在宏观上的光电转换的能力，定义为光电流 I_{ph} 与入射光功率 P_{opt} 的比值，表达式为 $SR=I_{ph}/P_{opt}$。光响应度与量子效率关系式为[26]：

$$SR = M\frac{\lambda}{1.24}QE \quad , \tag{13}$$

式中，M 为增益系数。根据式(12)定义的量子效率 QE，上式改写为：

$$SR = M\varphi(1-R)[1-\exp(-\alpha W_D)]\frac{\lambda}{1.24} \quad , \tag{14}$$

假设增益系数 M=1，φ=100%，根据式(14)计算得到可见光波段光响应度 SR 随耗尽层厚度 W_D 的变化关系，如图 5 所示。

图 5 中曲线表明，耗尽层厚度 W_D 分别为 1.0、2.0、3.0、4.0 与 5.0 μm 时，所对应的峰值光响应度 SR 分别约为 0.196、0.226、0.246、0.261 和 0.272 A·W^{-1}，相应的入射波长 λ 分别为 0.44、0.50、0.52、0.56 和 0.57 μm，与峰值量子效率所对应的入射波长相一致。

2.4 倍增层参数对增益的影响

光电流增益是 APD 最重要的特性，其根本物理机制是载流子的碰撞电离效应，通常用倍增系数表示。假设雪崩效应仅发生在倍增层，则在电子引发的雪崩情况下，倍增系数 $M_{(x)}$ 如式(15)所示[27]。由式(15)可知，雪崩倍增主要由耗尽层宽度、电场强度、载流子的碰撞离化系数等决定。

$$M_{(x)} = \frac{1}{1-\int_0^{W_m}\alpha(x)\exp(-\int_x^{W_m}[\alpha(x')-\beta(x')]\mathrm{d}x')\mathrm{d}x}, \tag{15}$$

式中，$\alpha(x)$ 和 $\beta(x)$ 分别为电子和空穴的碰撞离化系数，W_m 为倍增区厚度，Chynoweths 描述了电场强度 E 对载流子碰撞离化的影响，关系式为[28]：

$$\begin{cases}\alpha(x) = a_n\exp\left[-\left(\dfrac{b_n}{E(x)}\right)\right] \\ \beta(x) = a_p\exp\left[-\left(\dfrac{b_p}{E(x)}\right)\right]\end{cases} \quad , \tag{16}$$

式中，a_n, b_n, a_p, b_p 分别为电子和空穴的碰撞离化率的实验参数，$E(x)$ 是倍增区中电场强度，为距离 x 的函数。本文的数值计算采用 Lee 的实验拟合系数[29]：a_n=3.8×10^6 cm^{-1}，b_n=1.75×10^6 V·cm^{-1}；a_p=2.25×10^6 cm^{-1}，b_p=3.26×10^6 V·cm^{-1}。

考虑在一定掺杂浓度下，PN 结内倍增层的厚度、倍增层两侧的外加偏压 V_m 及倍增系数 M 三者之间的关系。假设 N 型衬底掺杂浓度为 N_D=1.0×10^{19} cm^{-3}，P 型倍增层掺杂浓度为 N_A=1.0×10^{16} cm^{-3}，结合公式(1)、(2)、(16)，为简化运算，将 $\alpha(x)$ 和 $\beta(x)$ 进行 3 阶泰勒展开，代入式(15)中，计算倍增层外加偏压 V_m 与倍增系数 M 的关系，结果如图 6(彩图见期刊电子版)所示。

图中曲线表明当倍增层两侧的外加偏压 V_m 增加至特定值时，M 急剧增加，公式(15)表明此时 V_m 大小接近或等于雪崩击穿时倍增层两侧的电压 $V_{br\text{-}m}$，因此，为了使 APD 获得较高增益，作用在器件的外加偏压 V_{apd} 大小需近似于器件的雪崩击穿电压 $V_{br\text{-}apd}$。图中曲线表明随着倍增层厚度的增加，获得相同倍增系数时的电压降低。即，在小的倍增层厚度下，需要提高电压，使载流子具有更高的电离率，才能获得较高的增益。但是倍增层厚度的增加受掺杂浓度和 PN 结两端外加偏压的影响，其厚度的选择还要依据电场分布选择，而电场分布又与掺杂浓度相关，因此倍增层的厚度需要与其掺杂浓度综合考虑。

对于硅，仅当电子能量 $E_{ele} \geqslant 6.5$ eV，载流子能量才完全损耗在碰撞电离过程中[30]，从能量角度分析，假设仅在倍增层发生碰撞电离效应，不考虑场控层对电子能量的影响，忽略空穴-电子复合机制及散射能量损耗，通过公式(4)可知，设载流子在倍增层的电场作用下获得能量 ΔE 为：

$$\Delta E = e\int_0^{W_m}\left(E_M - \frac{qN_p}{\varepsilon_0\varepsilon_p}x\right)\mathrm{d}x \quad . \tag{17}$$

为简便计算，将 PN 突变结击穿临近电场 E_m 代入上式整理得 ΔE：

$$\Delta E = e\int_0^{W_m}\left(\frac{4\times10^5}{1-(1/3)\log_{10}(N/10^{16})}-\frac{qN_p}{\varepsilon_0\varepsilon_p}x\right)dx = e\left(\frac{4\times10^5}{1-(1/3)\log_{10}(N/10^{16})}W_m-\frac{qN_p}{2\varepsilon_0\varepsilon_p}W_m^2\right) \quad . \tag{18}$$

设定衬底的掺杂浓度 N_{n++}=1.0×10^{19} cm^{-3}, 倍增层的掺杂浓度 N_p 为 1.0×10^{15}~1.0×10^{17} cm^{-3}, PN 结设为单边突变结, 根据公式(18)计算不同倍增层厚度下掺杂浓度与载流子获得能量 ΔE 的数值关系, 结果如图 7 所示。当倍增层厚度 W_m 固定为 0.5 μm 时, 由图 5 曲线可知, 掺杂浓度 N_p 分别为 1.2×10^{16}、1.8×10^{16} 与 2.4×10^{16} cm^{-3} 时, 能量 ΔE 分别为 18.22、18.39 与 18.26 eV。因此, 当倍增层掺杂浓度为 1.8×10^{16} cm^{-3} 时, 载流子在倍增层获得较高能量 ΔE=18.39 eV, 理论上可产生较高的增益系数 M。

2.5　场控层的影响

场控层的掺杂浓度(N_{p+})和厚度(W_c)是调节倍增层与吸收层电场过渡的重要参数, 场控层位于吸收层与倍增层之间, 通过降低吸收层的电场强度, 减少器件的隧穿几率。然而场控层厚度不宜过大, 原因如下: 当外加偏压与场控层掺杂浓度固定时, 增加场控层厚度会将减小吸收层的电场强度, 会影响吸收层光生载流子的漂移速度; 而厚度过小, 又会增加吸收层电场强度, 诱发载流子电离, 增加不必要的噪声电流。根据公式(5), 在保证载流子饱和漂移速度下, 选择合适的掺杂浓度和厚度, 有利于倍增层和吸收层之间电场的调节和过渡。一般地, 选择比倍增层小的厚度和比倍增层高的掺杂浓度, 可以保证对倍增层变化的影响最小。

2.6　吸收层设计

由于 Si 材料自身的吸收特性[31], 对波长为 0.4 ~ 0.5 μm 的蓝光波段具有较高的吸收系数(如图 3 所示), 导致蓝光波段的光在硅中的穿透深度较浅, 约为 0.098~0.82 μm。为了使蓝光被吸收层充分吸收, 结合图 4 所示的量子效率与耗尽层厚度的关系, 选取吸收层厚度 W_a=1.3 μm。在硅中, 当电场强度 E>1.0×10^4 V·cm^{-1} 时, 电子会趋于饱和漂移速度, v_s(Si)≈10^7 cm·s^{-1}。为了使器件保持较高的带宽, 载流子在器件中应以饱和速度运动。倍增层、场控层的掺杂浓度和厚度固定时(W_m=0.5 μm, N_p=1.8×10^{16} cm^{-3}; W_c=0.2 μm, N_{p+}=8.0×10^{16} cm^{-3}), 当突变 PN 结临近击穿时, 根据式(6)绘制了不同掺杂浓度下吸收层的场强分布, 如图 8(彩图见期刊电子版)所示。从图中可以看出, 吸收层的场强随着掺杂浓度的增加逐渐减小, 当吸收层的掺杂浓度为 N_π=1.0×10^{16} cm^{-3} 和 5.0×10^{15} cm^{-3} 时, 场强在到达表面非耗尽区以前已经耗尽, 此时蓝光激发的载流子进入吸收层以扩散运动为主, 增加了载流子的渡越时间, 降低了器件带宽。当 N_π 分别为: 1.0×10^{14} cm^{-3}、5.0×10^{14} cm^{-3} 和 1.0×10^{15} cm^{-3} 时, 吸收层的边缘场强 E>10^4 V·cm^{-1}, 器件处于拉通工作状态, 载流子在整个器件中以饱和速度漂移运动。所以吸收层的掺杂浓度和厚度选取需保证吸收层内载流子有良好的电场分布, 保证载流子的饱和漂移速度, 同时还要满足红绿光有一定的吸收率。

2.7　Si-APD 初始结构参数

假设各层掺杂均匀, 入射光仅在吸收层被吸收, 在反偏电压下, 雪崩效应只发生在倍增层。基于上文关于增益系数与外加偏压、倍增层厚度的关系、量子效率及光响应度与耗尽层厚度的关系, 选取的各层的参数如表 1 所示, 其中 W_s、W_a、W_c、W_m 和 W_{sub} 分别为表面非耗尽层、吸收层、场控层、倍增层和衬底的厚度。

3　Si-APD 数值计算

描述半导体器件工作的基本方程有: 静电方程、电流密度方程和连续性方程。载流子的产生与复合机制是影响半导体光电探测器性能的关键。对 Si-APD 的器件特性进行二维模拟, 计算采用的 Si-APD 的光敏面直径为 10 μm, 为了提高计算结果的准确性, 计算过程中采用了 Selberherr's 离化[32-33]、Shockley-Read-Hall 复合[34-35] 及载流子迁移率[36-38] 等物理模型。

3.1　Si-APD 的场强分布与外加偏压的关系

根据表 1 中的参数, 研究了器件中 V_{apd} 分别为: 0 V、0.5 $V_{br\text{-}apd}$、0.7 $V_{br\text{-}apd}$、$V_{br\text{-}apd}$(所对应的 V_{apd} 分别为: 0 V、17.1 V、23.9 V、34.2 V), Si-APD 内部的场强分布, 如图 9(彩图见期刊电子版)所示。从图中可以看出, Si-APD 内部的电场强度随着器件外加偏压 V_{apd} 的增加而提高。当 V_{apd} 较小时, 器件处于非拉通工作状态, 载流子在

器件中，开始以扩散运动为主，随着外加偏压的增加，器件整体被拉通，此时载流子以漂移运动为主，随着外加偏压的不断增加，载流子最终将以饱和漂移速度在器件中运动。

3.2 表面非耗尽层厚度进一步优化设计

通常半导体光电探测器表面具有一定厚度的表面重掺杂非耗尽层(兼作电极层)，蓝光波段的光在硅中的穿透深度较浅，当光经过器件顶部的非耗尽层时，大部分蓝光能量被该层吸收产生空穴—电子对，因此有必要对表面非耗尽层的厚度进行优化。在表 1 参数基础上，固定表面层的杂质浓度及其它掺杂层的结构参数，入射光垂直照射在探测器表面层，得到 $R\neq0$ 时，不同表面非耗尽层厚度的光谱响应曲线，结果如图 10(彩图见期刊电子版)所示。图中曲线展示了当表面非耗尽层厚度 W_s 分别为 0.03、0.06 和 0.10 μm 时，外加偏压为 0.95 $V_{br\text{-}apd}$ ($M\approx26$)下的光谱响应度，其中当 W_s=0.03 μm 时蓝光波段的光响应度 SR 为 3.71 ~ 6.08 A·W^{-1}；当 W_s=0.06 μm 时蓝光波段的光响应度为 SR 为 3.15~5.94 A·W^{-1}；当 W_s=0.10 μm 时蓝光波段光响应度为 SR 为 2.57~5.75 A·W^{-1}，表明表面非耗尽层越薄，对蓝光光响应度的抑制作用会越小。通过曲线也发现，W_s 的变化对器件在长波段入射光的光响应度的影响较小，分析认为根据光在介质中的传输特性，入射光在厚度为 W_s 的表面非耗尽层光吸收损耗 A_s 为：

$$A_s=(1-R)[1-\exp(-\alpha W_s)]\quad,\tag{19}$$

式中，R 为表面反射率，α 为 Si 的光吸收系数。宽度为 W_D 的耗尽区内光生载流子形成的漂移电流密度为：

$$J_{ph}=q\frac{(1-R)\exp(-\alpha W_S)P_{opt}}{A\cdot h\upsilon}\cdot[1-\exp(-\alpha W_D)].\tag{20}$$

可见光波段入射光功率 P_{opt} 固定，公式(20)的前半部分表示特定波长光透射至探测器的耗尽层边缘的光子数量，后半部分表征厚度为 W_D 的耗尽层对入射光子的吸收率，忽略载流子的复合机制，设耗尽区量子效率 QE=100%。根据 Si 的材料特性可知，长波段入射光被材料吸收的强度较小，因此表面非耗尽层产生的光吸收损耗对透射至耗尽层的光能量影响较小，因此调节 W_s 的过程中长波段光响应度基本稳定。但在短波一侧，表面非耗尽层厚度对光响应度有较大的影响。

3.3 倍增层的掺杂浓度对光响应度的影响

根据图 10 的计算结果，结合上面非表面耗尽层厚度计算结果，取表面非耗尽层厚度 W_s=0.03 μm，表面反射率 $R\neq0$，其它参数依据表 1 中数据，得到 V_{apd}=0.95$V_{br\text{-}apd}$ 时，Si-APD 在可见光波段的光响应度如图 11(彩图见期刊电子版)红色曲线所示，所对应的蓝光波段的光响应度分为 SR=3.72~6.08 A·W^{-1}。

作为比较，在其他参数不变的情况下，还分别计算了倍增层掺杂浓度 N_p 分别为 1.2×10^{16} cm^{-3}、2.4×10^{16} cm^{-3}(所对应的击穿电压 $V_{br\text{-}apd}$分别为 39.2 V、30 V)，V_{apd}=0.95 $V_{br\text{-}apd}$ 时的光响应度，如图 11 中蓝线和黑线所示，所对应的蓝光波段的光响应度 SR 分别为 3.02~4.93 A·W^{-1}、2.83~4.68 A·W^{-1}。这两种情况下，光响应度均低于红线所示的 N_p=1.8×10^{16} cm^{-3} 掺杂时的 SR 值。

这种现象可以归因于在该掺杂浓度下，载流子在倍增层可以获得更高的能量(如图 7 所示)，产生更大的光电流增益。根据上述的研究结果，最终确定 Si 光探测器的基本外延结构参数如表 2 所示。

3.4 Si-APD 暗电流的 I-V 特性

假定每一层都是均匀掺杂的，Si-APD 在暗环境中的 I-V 关系特性可以反映器件的雪崩击穿电压 $V_{br\text{-}apd}$、电流增益系数 M 等电学参数。根据表 2 中参数及公式(21)定义的电流密度方程定性计算 I-V 特性曲线。电流密度大小主要受载流子输运行为的影响，在数值关系上表示为电子电流密度和空穴电流密度之和，即：

$$\begin{cases}J_n=qn\mu_nE+qD_n\nabla n\\J_p=qp\mu_pE-qD_p\nabla p\\J_{cond}=J_n+J_p\end{cases}\quad,\tag{21}$$

式中 J_n 为电子电流密度，J_p 为空穴电流密度，J_{cond} 为传导电流密度，μ_n 为电子迁移率，μ_p 为空穴迁移率，D_n 为电子扩散系数，D_p 为空穴扩散系数，∇n、∇p为过剩载流子浓度梯度。图 12 中曲线展示了计算得到的反向电流与外加偏压 V_{apd} 的变化关系。从图中可以看出电流大小随 V_{apd} 的增加而不断提高，但电流的变化趋势不同，根据不同的电流形成机理，总结为图 12 中 (i)−(iv) 部分。

雪崩光电二极管的暗电流密度包括[39]复合电流密度 J_r，少子扩散电流密度 J_{diff}，耗尽层的载流子漂移电流密度 J_{dr} 与雪崩电流密度 J_m。复合电流密度表示为 $J_r=qn_iW_D/2\tau_D$。$\tau_D=1/R_{ec}\cdot N$，为载流子寿命，$R_{ec}\approx10^{-15}$ cm³s⁻¹，为间接带隙半导体复合系数[27]，N 为掺杂浓度。$J_{diff}=(qD_pn_i^2/L_pN_D)+(qD_nn_i^2/L_nN_A)$，$D_p=kT\mu_p/q$ 与 $D_n=kT\mu_n/q$ 分别为空穴与电子扩散系数，L_p 和 L_n 分别为空穴与电子的扩散长度。当 T=300 K 时，kT/q=0.0259 V，D_p=12.95 cm²·s⁻¹，D_n=37.56 cm²·s⁻¹。为简便计算，结合上文设计的 APD 结构中 π 吸收层、p+型场控层与 p 型倍增层的掺杂浓度，将该 3 个区域视为掺杂浓度 $\overline{N_A}$、载流子寿命 $\overline{\tau_{sc}}$ 的 P 型硅材料：

$$\overline{N_{\mathrm{A}}}=\frac{N_{\mathrm{p}}+N_{\mathrm{p+}}+N_{\pi}}{3}=3.3\times10^{16}\ \mathrm{cm^{-3}}\quad,\qquad(22)$$

$$\overline{\tau_{\mathrm{sc}}}=\frac{\tau_{\mathrm{sc(p)}}+\tau_{\mathrm{sc(p^+)}}+\tau_{\mathrm{sc(\pi)}}}{3}=0.356\ \mathrm{s}\quad,\qquad(23)$$

$\tau_{sc(p)}$，$\tau_{sc(p+)}$ 与 $\tau_{sc(\pi)}$ 分别为倍增层、场控层与吸收层的载流子寿命。

当外加偏压 V_{apd} 较小时，Si-APD 电流以扩散电流和复合电流为主。将上述数据代式(24)计算器件的扩散与复合电流，结果对应于图 12 的 (i) 部分。

$$I_{(i)}=\int_0^{W_D}(J_r+J_{\mathrm{diff}})\,\mathrm{d}x\quad.\qquad(24)$$

增加外加偏压 V_{apd}，受内部电场作用的载流子数量增多，漂移电流为电流的主要部分，根据式(21)，器件的漂移电流密度表示为：$J_{dr}=qn\mu_nE+qp\mu_pE$，其中 E 为式(4)~(7)定义的耗尽层电场强度，将计算结果 J_{dr} 代入下式(25)，结果对应于图 12 中 (ii) 部分。

$$I_{(ii)}=\int_0^{W_D}\left(qn\mu_nE+qp\mu_pE\right)\mathrm{d}x\quad.\qquad(25)$$

若外加偏压 V_{apd} 持续增加，载流子在强电场作用下发生碰撞电离，高能初始载流子撞击内部晶格产生次生载流子，之后继续碰撞晶格产生新的载流子，形成雪崩电流密度 $J_m=(\alpha_nJ_n+\alpha_pJ_p)$，$J_n$ 与 J_p 为电子与空穴电流密度，α_n、α_p 分别为电子和空穴的离化系数。该碰撞效应在工作偏压下持续进行，载流子数量倍增，假设雪崩效应仅在倍增层内发生，则厚度为 W_m 的倍增层内产生的雪崩暗电流 I_d 可以表示为：

$$I_{\mathrm{d}}=\int_0^{W_{\mathrm{m}}}\left(\alpha_{\mathrm{n}}J_{\mathrm{n}}+\alpha_{\mathrm{p}}J_{\mathrm{p}}\right)\mathrm{d}x\quad.\qquad(26)$$

如图 12 的第(iii)部分所示。

通常，器件的增益系数 M 可根据经验关系式 (27) 得出

$$M=\frac{I_{\mathrm{d}}}{I_{\mathrm{d_0}}}=\frac{1}{1-\left(\dfrac{V_{\mathrm{apd}}}{V_{\mathrm{br-apd}}}\right)^n}\quad,\qquad(27)$$

式中，I_d 为基于载流子激发碰撞电离作用下产生的电流，I_{d0} 为初始暗电流，常量 n 大小受器件结构、掺杂分布等因素影响，通常 Si 材料的 n 为 1.5~4.0。当外加偏压 V_{apd} 接近雪崩击穿电压 $V_{br\text{-}apd}$ 时，则此时电流会随倍增因子 M 急剧增加而提高，如图 12 中区域 (iv) 所示。

图 12 的暗电流 I-V 关系曲线表明：APD 器件处于低外加偏压时，扩散电流占总电流的主要部分；之后内部电场强度随 V_{apd} 增加而提高，耗尽区宽度增大，更多的载流子进入耗尽区，在电场作用下形成漂移电流，其成为总电流的主要部分；当 V_{apd} 持续增加，由于载流子碰撞电离作用，出现电流增益现象但效果不明显；若 V_{apd} 接近器件雪崩击穿电压 $V_{br\text{-}apd}$，则出现电流急剧增加现象。

通过对比(iii)与(iv)部分中的电流随电压的变化趋势发现，APD 处于相对雪崩击穿电压较高的偏压时可产生较高的电流增益 M。分析认为载流子的离化率是衡量雪崩倍增效应的重要指标，其与器件偏压相关联的电场强度联系紧密[40]，离化率随偏压提高而增大。以在倍增层内的电子为例，根据(16)式并按照 *Lee* 的载流子电离参数与(4)式的电场分布计算电子、空穴在不同偏压下的碰撞电离率分布，图 13(a)和图 13(b)(彩图见期刊电子版)清楚表明碰撞离化系数随倍增层两侧电压 V_m 的增加而提高，因此在 V_{apd} 接近 $V_{br\text{-}apd}$ 时会出现电流高增益现象，并且以电子增益为主。

4　结　论

为了解决光通信系统对蓝光高响应光电探测器的迫切需求，本文设计了一种吸收层与倍增层互换位置 SACM 型 Si-APD 结构，研究了倍增层

厚度与器件增益、吸收层掺杂浓度与吸收层场强分布、外加偏压与器件内部场强分布、表面非耗尽层厚度与光谱响应度以及倍增层浓度与光谱响应的关系，综合考虑，选取器件的结构参数为：表面非耗尽层厚度为 0.03 μm，掺杂浓度 1.0×10^{18} cm^{-3}；吸收层厚度为 1.3 μm，掺杂浓度为 1.0×10^{15} cm^{-3}；场控层厚度为 0.2 μm，掺杂浓度 8.0×10^{16} cm^{-3}；倍增层厚度为 0.5 μm，掺杂浓度为 1.8×10^{16} cm^{-3}。该器件具有较低的击穿电压 $V_{br\text{-}apd}$=34.2 V，当 V_{apd}=0.95 $V_{br\text{-}apd}$ 在蓝光波段有较高的光响应度 SR=3.72~6.08 A·W^{-1}。本文的研究结果对实际器件的制备具有一定参考价值。

References:

[1] 邓健志，程小辉. 可见光车灯信号发送控制装置[J]. 光学 精密工程，2020，28(12)：2710-2718.
DENG J ZH, CHENG X H. Visible light vehicle lamp signal transmission control device[J]. *Optics and Precision Engineering*, 2020, 28(12): 2710-2718. (in Chinese)

[2] 董冰，佟首峰，张鹏，等. 20 m水下无线蓝光LED通信系统样机设计[J]. 中国光学，2021，14(6)：1451-1458.
DONG B, TONG SH F, ZHANG P, *et al*.. Design of a 20 m underwater wireless optical communication system based on blue LED[J]. *Chinese Optics*, 2021, 14(6): 1451-1458. (in Chinese)

[3] 刘洋，蔡喜平，林朗，等. LED可见光通信网络与以太网互融技术的研究[J]. 光通信技术，2019，43(1)：1-4.
LIU Y, CAI X P, LIN L, *et al*.. Research on the fusion technology of LED visible optical communication network with Ethernet[J]. *Optical Communication Technology*, 2019, 43(1): 1-4. (in Chinese)

[4] 徐宪莹，岳殿武. 可见光通信中正交频分复用调制技术[J]. 中国光学，2021，14(3)：516-527.
XU X Y, YUE D W. Orthogonal frequency division multiplexing modulation techniques in visible light communication[J]. *Chinese Optics*, 2021, 14(3): 516-527. (in Chinese)

[5] 周政，缪文南，李亚，等. 可见光通信中GaN-LED PN结面积对调制带宽的影响机理[J]. 光学 精密工程，2020，28(7)：1494-1499.
ZHOU ZH, MIAO W N, LI Y, *et al*.. Influence mechanism of GaN-LED's PN junction area on modulation bandwidth in visible light communication[J]. *Optics and Precision Engineering*, 2020, 28(7): 1494-1499. (in Chinese)

[6] 周青超，柏泽龙，鲁路，等. 白光LED远程荧光粉技术研究进展与展望[J]. 中国光学，2015，8(3)：313-328.
ZHOU Q CH, BAI Z L, LU L, *et al*.. Remote phosphor technology for white LED applications: advances and prospects[J]. *Chinese Optics*, 2015, 8(3): 313-328. (in Chinese)

[7] 陈雄斌，闵成彧. 看得见的无线通信技术——可见光通信[J]. 物理，2020，49(10)：688-696.
CHEN X B, MIN CH Y. Wireless communication that we can see——visible light communication[J]. *Physics*, 2020, 49(10): 688-696. (in Chinese)

[8] 高绪敏. 面向可见光通信的硅基氮化物同质光电子集成芯片研究[D]. 南京：南京邮电大学，2018.
GAO X M. *Study on silicon based nitride homologous optoelectronic integrated chip for visible light communication*[D]. Nanjing: Nanjing University of Posts and Telecommunications, 2018. (in Chinese)

[9] ZIMMERMANN R, BRAUN F, ACHTNICH T, *et al*.. Silicon photomultipliers for improved detection of low light levels in miniature near-infrared spectroscopy instruments[J]. *Biomedical Optics Express*, 2013, 4(5): 659-666.

[10] 魏佳童. 基于硅和锗的新型 APD 结构设计与研究[D]. 哈尔滨：哈尔滨工程大学，2016.
WEI J T. *The structure design and research of new type APD based on silicon and germanium*[D]. Harbin: Harbin Engineering University, 2016. (in Chinese)

[11] 朱晓秀，葛咏，李建军，等. 量子点增强硅基探测成像器件的研究进展[J]. 中国光学，2020，13(1)：62-74.
ZHU X X, GE Y, LI J J, *et al*.. Research progress of quantum dot enhanced silicon-based photodetectors[J]. *Chinese Optics*, 2020, 13(1): 62-74. (in Chinese)

[12] 王艺蒙，舒浩文，韩秀友. 高精度硅基集成光学温度传感器研究[J]. 中国光学，2021，14(6)：1355-1361.
WANG Y M, SHU H W, HAN X Y. High-precision silicon-based integrated optical temperature sensor[J]. *Chinese Optics*, 2021, 14(6): 1355-1361. (in Chinese)

[13] MOLL J L, VAN OVERSTRAETEN R. Charge multiplication in silicon p-n junctions[J]. *Solid-State Electronics*, 1963, 6(2): 147-157.

[14] PEPIN C M, DAUTET H, BERGERON M, *et al*.. New UV-enhanced, ultra-low noise silicon avalanche photodiode for radiation detection and medical imaging[C]. *IEEE Nuclear Science Symposuim & Medical Imaging Conference*, IEEE, 2010: 1740-1746.

[15] OTHMAN M A, YASIN N Y M, ARSHAD T S M, *et al*.. Variable intrinsic region in CMOS PIN photodiode for I–V characteristic analysis[C]. *Proceedings of the 1st International Conference on Communication and Computer Engineering*, Springer, 2015: 95-101.

[16] 王旭东. 硅基 APD 近紫外探测增强的结构优化研究[D]. 哈尔滨: 哈尔滨工业大学, 2015.
WANG X D. *Optimization of the enhancement of the Si-based APD for near-ultraviolet detection through structural design*[D]. Harbin: Harbin Institute of Technology, 2015. (in Chinese)

[17] 霍林章, 谭何盛, 何燃, 等. 蓝紫光增强硅光电倍增器的研究[J]. 激光与光电子学进展, 2015, 52(11): 110401.
HUO L ZH, TAN H SH, HE R, *et al*.. Research of blue-violet enhanced silicon photomultiplier[J]. *Laser & Optoelectronics Progress*, 2015, 52(11): 110401. (in Chinese)

[18] 鲁欢欢. 可见光通信硅基蓝光增强 APD 探测器仿真研究 [D]. 广州: 暨南大学, 2019.
LU H H. *Simulation study on silicon-based blue-light enhanced APD detector for visible light communication*[D]. Guangzhou: Jinan University, 2019. (in Chinese)

[19] SCHINKE C, PEEST P C, SCHMIDT J, *et al*.. Uncertainty analysis for the coefficient of band-to-band absorption of crystalline silicon[J]. *AIP Advances*, 2015, 5(6): 067168.

[20] 陈锋. 可见光通信 APD 探测器的蓝光增强技术研究[D]. 长春: 长春理工大学, 2018.
CHEN F. *The enhancement of the APD for Blu-Ray detection in VLC*[D]. Changchun: Changchun University of Science and Technology, 2018. (in Chinese)

[21] 王浩冰. 硅基雪崩光电二极管蓝光增敏研究[D]. 北京: 中国科学院大学(中国科学院长春光学精密机械与物理研究所), 2020.
WANG H B. *Research on enhancement in blue-light properties of silicon based avalanche photodiode*[D]. Beijing: University of Chinese Academy of Sciences (Changchun Institute of Optics, Precision Machinery and Physics, Chinese Academy of Sciences), 2020. (in Chinese)

[22] 史衍丽, 朱泓遐, 杨雪艳, 等. InP基自由运行模式单光子APD[J]. 红外与激光工程, 2020, 49(1): 0103005.
SHI Y L, ZHU H X, YANG X Y, *et al*.. InP-based free running mode single photon avalanche photodiode[J]. *Infrared and Laser Engineering*, 2020, 49(1): 0103005. (in Chinese)

[23] 刘恩科, 朱秉升, 罗晋生. 半导体物理学[M]. 7版. 北京: 电子工业出版社, 2017: 66-67.
LIU E K, ZHU D SH, LUO J SH. *Physics of Semiconductors*[M]. 7th ed. Beijing: Publishing House of Electronics Industry, 2017: 66-67. (in Chinese)

[24] CHYNOWETH A G. Chapter 4 charge multiplication phenomena[J]. *Semiconductors and Semimetals*, 1968, 4: 263-325.

[25] 杨孟. 空间量子通信硅雪崩光电二极管单光子探测器技术研究[D]. 合肥: 中国科学技术大学, 2019.
YANG M. *The research of silicon avalanche photodiode single photon detector on space quantum communication*[D]. Hefei: University of Science and Technology of China, 2019. (in Chinese)

[26] 李媛. 雪崩光电二极管的性能测试与仿真优化设计[D]. 武汉: 华中科技大学, 2017.
LI Y. *Theoretical and experimental study on avalanche photodiodes and optimization design*[D]. Wuhan: Huazhong University of Science and Technology, 2017. (in Chinese)

[27] 施敏, 伍国钰. 半导体器件物理[M]. 耿莉, 张瑞智, 译. 3版. 西安: 西安交通大学出版社, 2008.
SZE S M, NG K K. *Physics of Semiconductor Devices*[M]. GENG L, ZHANG R ZH, trans. 3rd ed. Xi'an: Xi'an Jiaotong University Press, 2008. (in Chinese)

[28] WOODS M H, JOHNSON W C, LAMPERT M A. Use of a Schottky barrier to measure impact ionization coefficients in semiconductors[J]. *Solid-State Electronics*, 1973, 16(3): 381-394.

[29] FOSSUM J G, MERTENS R P, LEE D S, *et al*.. Carrier recombination and lifetime in highly doped silicon[J]. *Solid-State Electronics*, 1983, 26(6): 569-576.

[30] OLDHAM W G, SAMUELSON R R, ANTOGNETTI P. Triggering phenomena in avalanche diodes[J]. *IEEE*

Transactions on Electron Devices, 1972, 19(9): 1056-1060.

[31] GAO D, ZHANG J, WANG F, *et al*.. Design and simulation of ultra-thin and high-efficiency silicon-based trichromatic PIN photodiode arrays for visible light communication[J]. *Optics Communications*, 2020, 475: 126296.

[32] VAN OVERSTRAETEN R, DE MAN H. Measurement of the ionization rates in diffused silicon *p-n* junctions[J]. *Solid-State Electronics*, 1970, 13(5): 583-608.

[33] SELBERHERR S. *Analysis and Simulation of Semiconductor Devices*[M]. Vienna: Springer, 1984.

[34] HALL R N. Electron-hole recombination in germanium[J]. *Physical Review*, 1952, 87(2): 387.

[35] SHOCKLEY W, READ JR W T. Statistics of the recombinations of holes and electrons[J]. *Physical Review*, 1952, 87(5): 835-842.

[36] ARORA N D, HAUSER J R, ROULSTON D J. Electron and hole mobilities in silicon as a function of concentration and temperature[J]. *IEEE Transactions on Electron Devices*, 1982, 29(2): 292-295.

[37] CAUGHEY D M, THOMAS R E. Carrier mobilities in silicon empirically related to doping and field[J]. *Proceedings of the IEEE*, 1967, 55(12): 2192-2193.

[38] MASETTI G, SEVERI M, SOLMI S. Modeling of carrier mobility against carrier concentration in arsenic-, phosphorus-, and boron-doped silicon[J]. *IEEE Transactions on Electron Devices*, 1983, 30(7): 764-769.

[39] FORREST S. Performance of InxGa1-xAsyP1-yphotodiodes with dark current limited by diffusion, generation recombination, and tunneling[J]. *IEEE Journal of Quantum Electronics*, 1981, 17(2): 217-226.

[40] 顾怀奇. Si 基微元 APD 雪崩增益与结构参数优化化的研究[D]. 哈尔滨: 哈尔滨工业大学, 2012.
GU H Q. *The study of avalanche gain and structural parameter optimization in Si based micro-pixel APD*[D]. Harbin: Harbin Institute of Technology, 2012. (in Chinese)

Author Biographics:

CHEN Wei-shuai (1994—), male, from Liaocheng, Shandong province, graduated from Shandong Jianzhu University in 2018 with a Bachelor of Science degree. Now he is a PhD student of Changchun Institute of Optics, Fine Mechanic and Physics, Chinese Academy of Sciences. He is mainly engaged in the research of nanophotonics and semiconductor photodetectors. E-mail: chenws159@163.com

陈伟帅(1994—),男,山东聊城人,2018 年于山东建筑大学获得理学学士学位,现为中国科学院长春光学精密机械与物理研究所博士研究生。主要从事纳米光子学与半导体光电探测器方面的研究。E-mail: chenws159@163.com

WANG Hao-bing (1994—), male, born in Songyuan, Jilin, master degree, in 2020, received a master degree from Changchun Institute of Optics, Fine Mechanics and Physics, Chinese Academy of Sciences (now he is in University of Technology of Troyes (France) - University of Reims (France) to continue his studies). His research interests include nanophotonics and semiconductor photodetectors. E-mail: 996490955@qq.com

王浩冰(1994—),男,吉林松原人,硕士,2020 年于中国科学院长春光学精密机械与物理研究所获得硕士学位(现在法国特鲁瓦工程技术大学—法国兰斯大学继续学习)。主要从事纳米光子学与半导体光电探测器方面的研究。E-mail: 996490955@qq.com

Liang Jingqiu (1962—), female, born in Changchun, Jilin Province, Ph.D., researcher, doctoral supervisor, received a Ph.D. from Changchun Institute of Optics, Fine Mechanics and Physics, Chinese Academy of Sciences in 2003, and is currently a researcher at Changchun Institute of Optics, Fine Mechanics and Physics, Chinese Academy of Sciences. She is mainly engaged in micro/nano optical structure, device and system research, infrared spectroscopy/imaging spectroscopy technology and infrared optical instrument research, micro LED micro display chip and application research and visible light communication device and system research. E-mail: liangjq@ciomp.ac.cn

梁静秋（1962—），女，吉林长春人，博士，研究员，博士生导师，2003 年于中国科学院长春光学精密机械与物理研究所获得博士学位，现为中国科学院长春光学精密机械与物理研究所研究员。主要从事微/纳光学结构、器件与系统研究、红外光谱/成像光谱技术及红外光学仪器研究、micro LED 微显示芯片及应用研究与可见光通信器件及系统方面的研究。E-mail: liangjq@ciomp.ac.cn

Wang Wei-biao (1962—), male, born in Yangzhou, Jiangsu, Ph.D., researcher, doctoral supervisor, received a Ph.D. from Changchun Institute of Optics, Fine Mechanics and Physics, Chinese Academy of Sciences in 1999, and now he is a researcher at Changchun Institute of Optics, Fine Mechanics and Physics, Chinese Academy of Sciences. His research interests include optoelectronic materials and devices, photodetectors, LED array chip integration and applications, photonic crystals, micro-nano photonics, field emission materials and electron emission characteristics. E-mail: wangwb@ciomp.ac.cn

王惟彪（1962—），男，江苏扬州人，博士，研究员，博士生导师，1999 年于中国科学院长春光学精密机械与物理所获博士学位，现为中国科学院长春光学精密机械与物理研究所研究员。主要从事光电子材料与器件、光电探测器、发光二极管（LED）阵列芯片集成及应用、光子晶体、微纳光子学、场发射材料与电子发射特性等方面的研究。E-mail: wangwb@ciomp.ac.cn